

SUPPORTING INFORMATION

Iridium complexes catalysed selective dehydrogenation of glucose to gluconic acid in water

*Pilar Borja,^a Cristian Vicent,^b Miguel Baya,^c Hermenegildo García,^{*d} and Jose A. Mata^{*a}*

^aInstitute of Advanced Materials (INAM), Universitat Jaume I, Avda. Sos Baynat s/n, 12071, Castellón (Spain). Fax: (+34) 964387522; Tel: (+34) 964387516; e-mail: jmata@uji.es

^bServeis Centrals d'Instrumentació Científica (SCIC). Universitat Jaume I, Avda. Sos Baynat s/n, 12071, Castellón (Spain)

^cInstituto de Síntesis Química y Catálisis Homogénea (ISQCH), Departamento de Química Inorgánica, CSIC-Universidad de Zaragoza, C/Pedro Cerbuna 12, E-50009 Zaragoza (Spain)

^dInstituto de Tecnología Química (ITQ), Universidad Politécnica de Valencia. Avda. Los Naranjos s/n, 46022, Valencia (Spain)

Contents

S1. Experimental section.....	3
S2. Nuclear Magnetic Resonance (NMR) Analysis.....	3
S2.1 ¹ H NMR spectrum of complex (1) in CDCl ₃ :	3
S2.2 NMR characterization of complex (2).....	4
S2.3 ¹ H NMR spectrum of complex IrCp*(NHC)(H ₂ O) ₂ (3) in D ₂ O:.....	6
S2.4 ¹ H NMR spectra of Glucose, Gluconic acid and the mixture in basic D ₂ O.	7
S2.5 NMR characterization of complex (4).....	8
S3. HPLC-ESI-MS/MS method for the quantification of glucose and gluconic acid.....	10
S3.1. Preparation of the calibration standards	10
S3.2. Instrumentation, MS/MS optimization and chromatography.....	11
S3.3. Study of matrix effects	12
S3.4. Sample preparation	13
S3.5. References.....	13
S3.6. HPLC reaction monitoring data of table 1.	14
S4. X-Ray Diffraction Studies	19
S5. Electrospray Ionization Mass Spectrometry (ESI-MS) and Collision Induced Dissociation (CID) experiments.	28
S6. Speciation of complex 1 in H ₂ O by ¹ H NMR spectroscopy.....	30
S7. Density Functional Theory (DFT) calculations	31

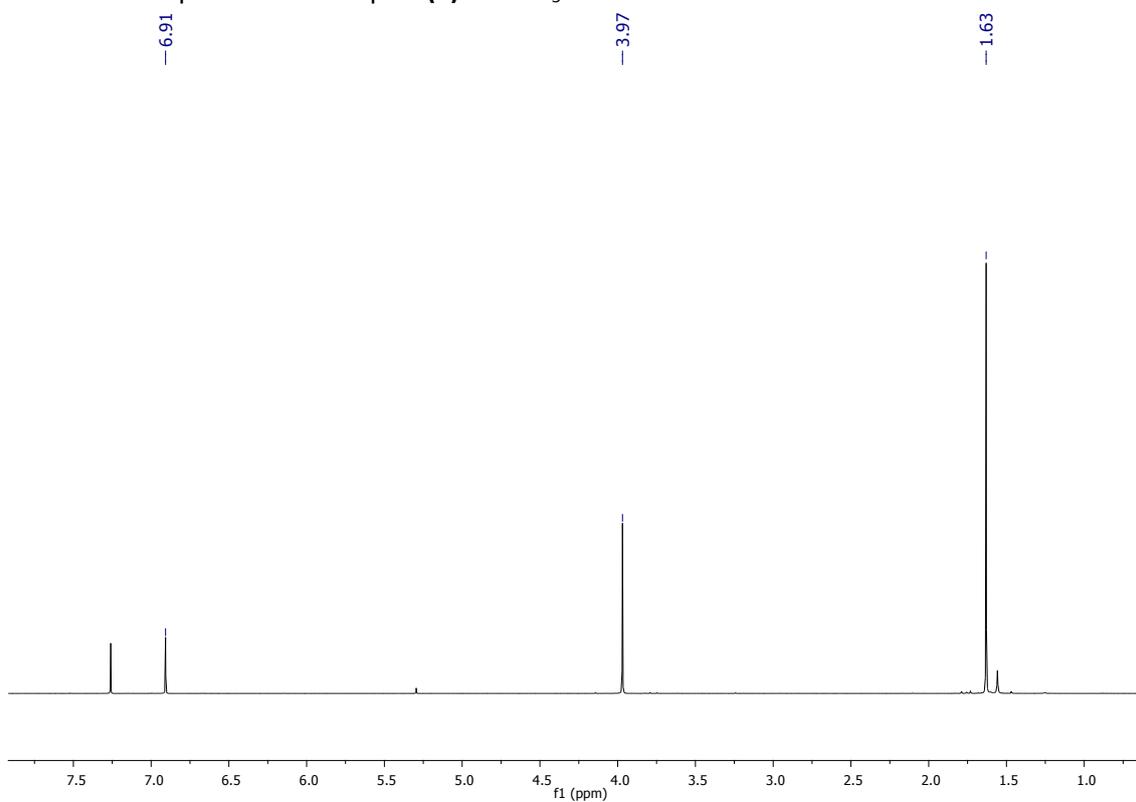
S7.1 Computational details	31
S7.2 Computational considerations	31
S7.3 Equilibria between iridium species present under the reaction conditions.....	32
S7.4 Mechanism proposal and calculated energy profile.	32
S7.5 References.....	35

S1. Experimental section

General procedures: D-Glucose (99 %), D-Gluconic acid (50 % aq. sol), and Ag_2SO_4 (99 %) were purchased from commercial suppliers and used as received. HPLC-grade methanol (MeOH), formic acid (HCOOH, content >98%) were purchased from Scharlab (Barcelona, Spain). HPLC-grade water was obtained from distilled water passed through a Milli-Q water purification system (Millipore, Bedford, MA, USA). Nuclear magnetic resonance (NMR) spectra were recorded on Bruker spectrometers operating at 300 or 400 MHz (^1H NMR) and 75 or 100 MHz ($^{13}\text{C}\{^1\text{H}\}$ NMR), respectively, and referenced to SiMe_4 (δ in ppm and J in Hz). NMR spectra were recorded at room temperature with the appropriate deuterated solvent.

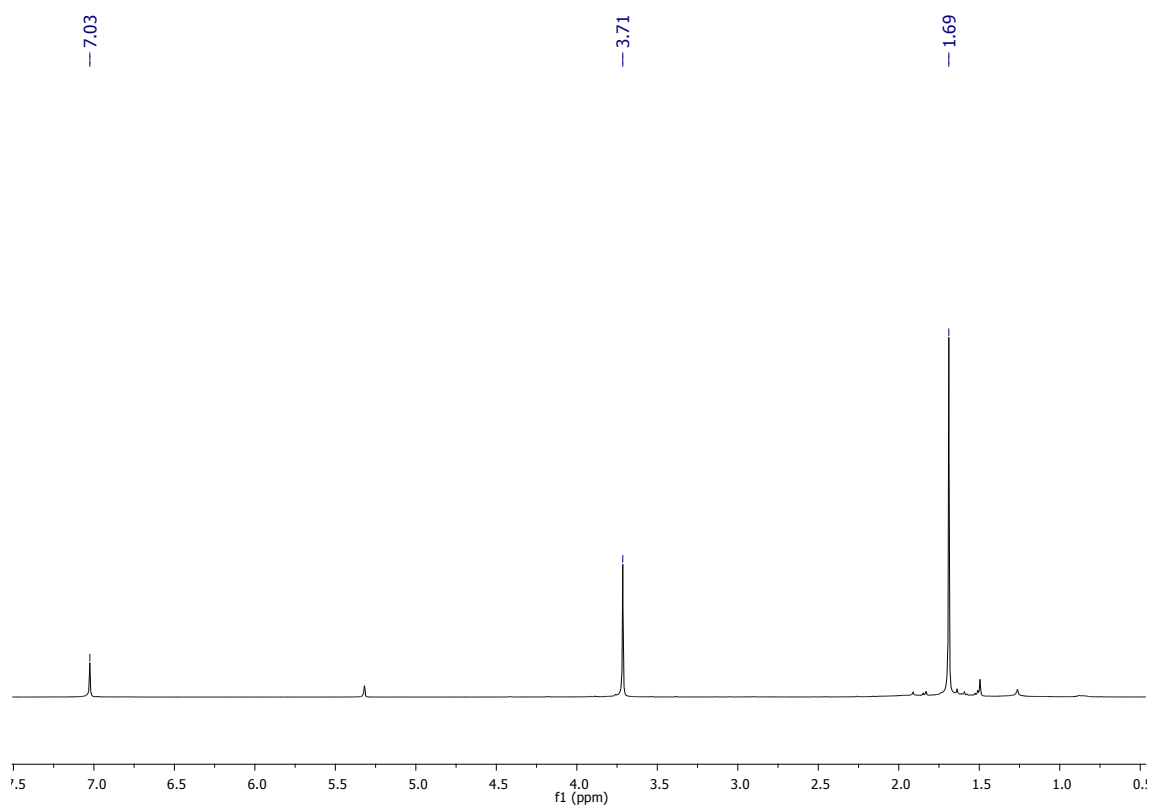
S2. Nuclear Magnetic Resonance (NMR) Analysis

S2.1 ^1H NMR spectrum of complex **(1)** in CDCl_3 :

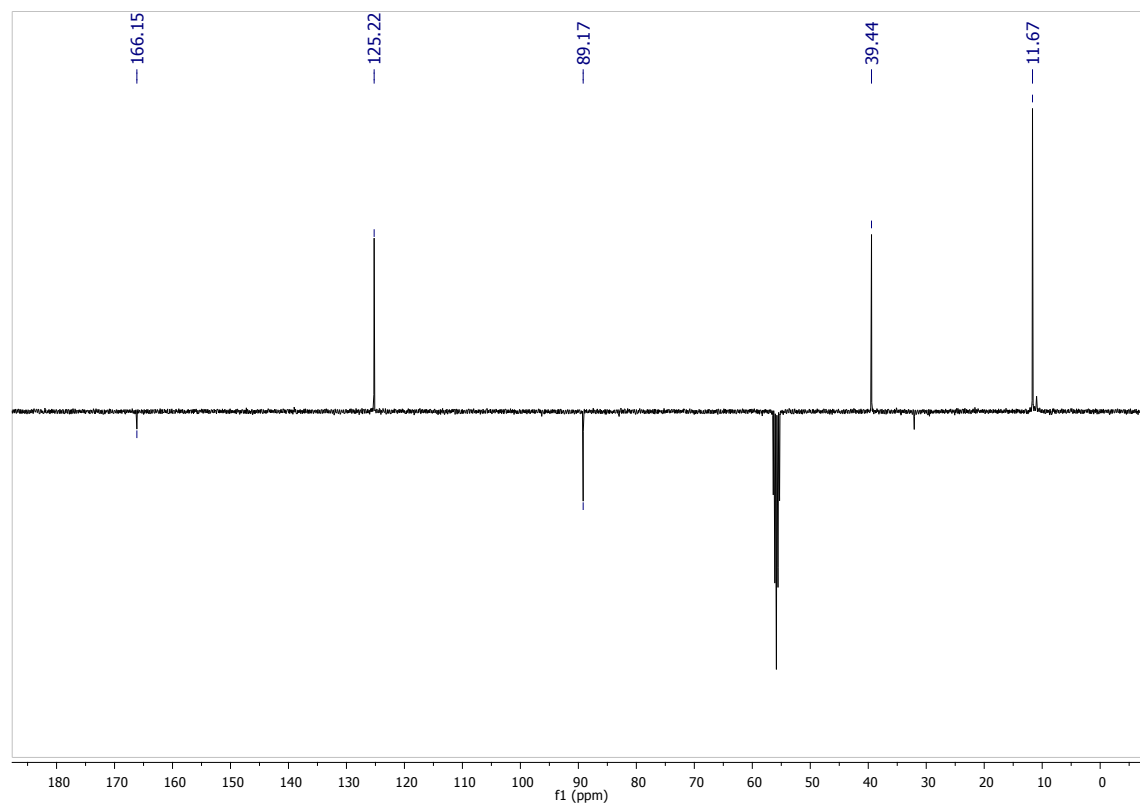


S2.2 NMR characterization of complex **(2)**.

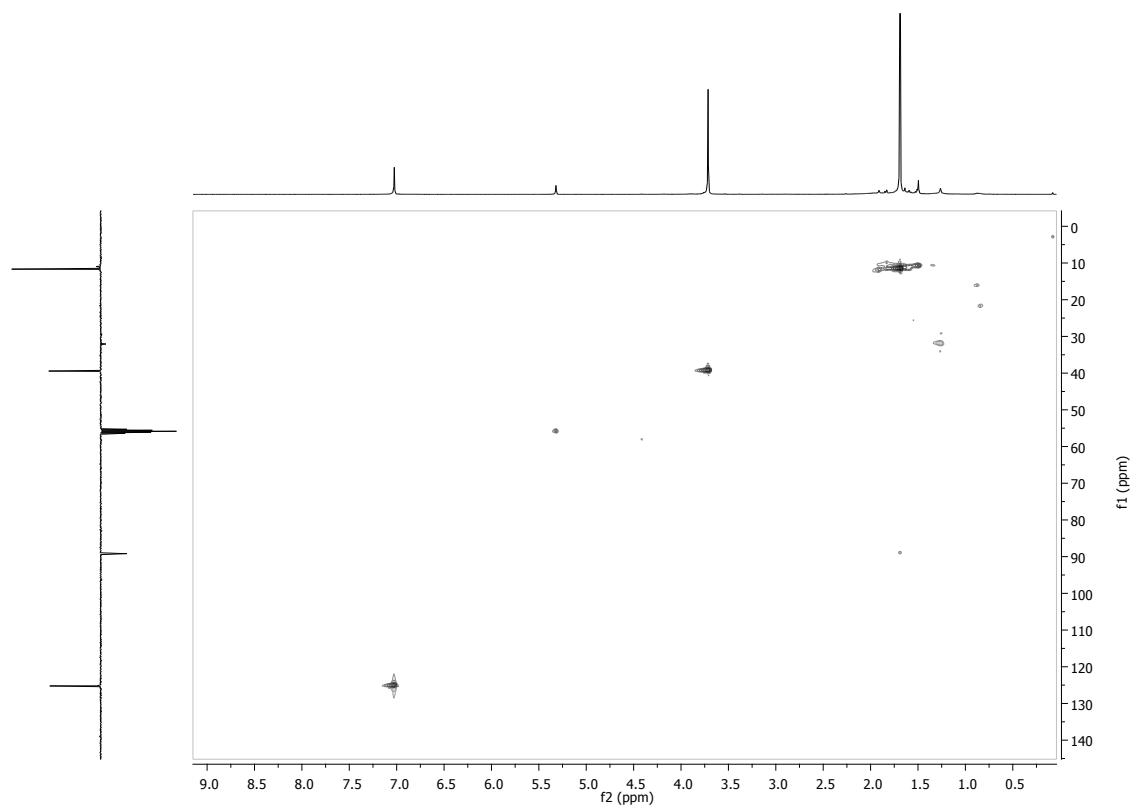
^1H NMR spectrum of complex **(2)** in CD_2Cl_2 :



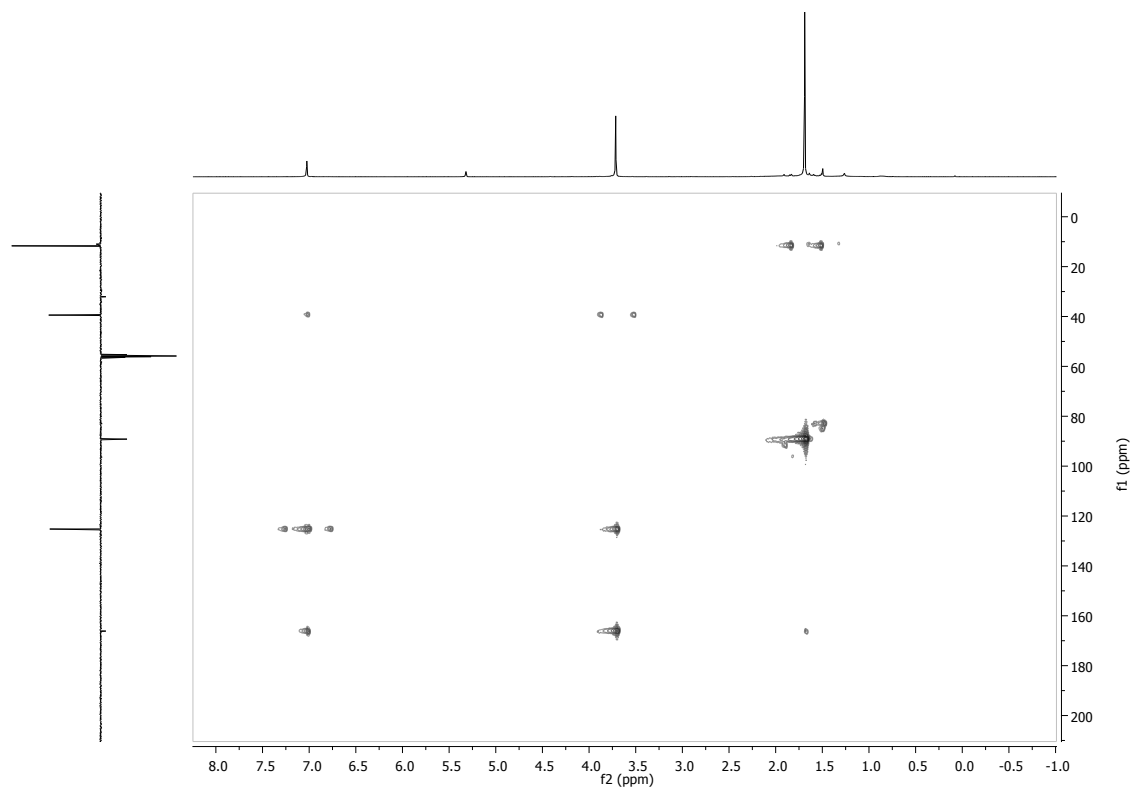
APT of complex **(2)** in CD_2Cl_2 :



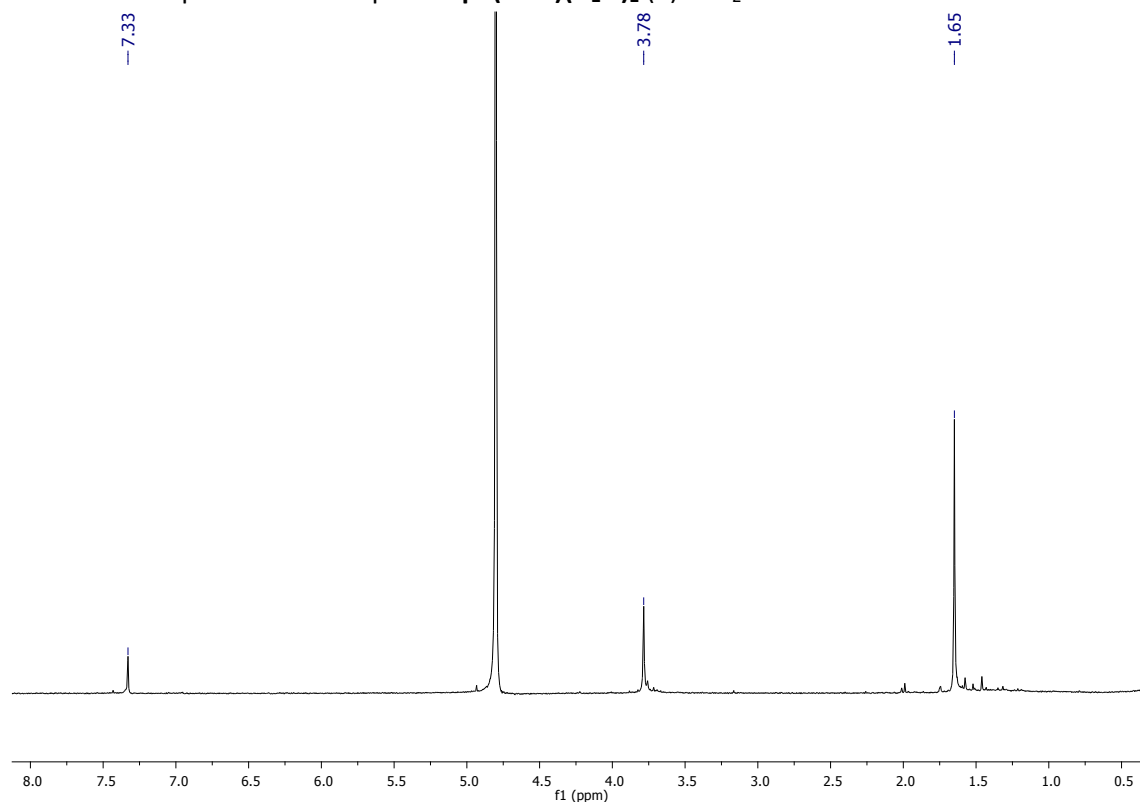
^1H - ^{13}C -HSQCed of complex (2) in CD_2Cl_2 :



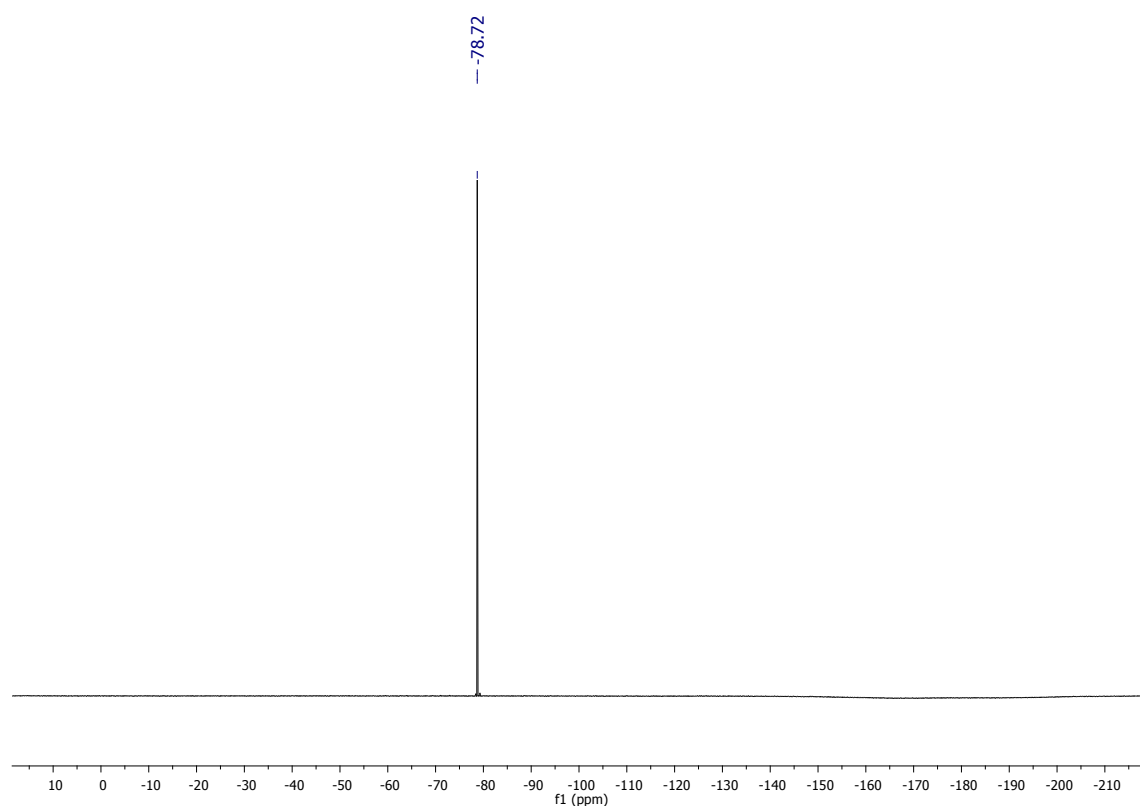
^1H - ^{13}C -HMBC of complex (2) in CD_2Cl_2 :



S2.3 ^1H NMR spectrum of complex $\text{IrCp}^*(\text{NHC})(\text{H}_2\text{O})_2$ (**3**) in D_2O :

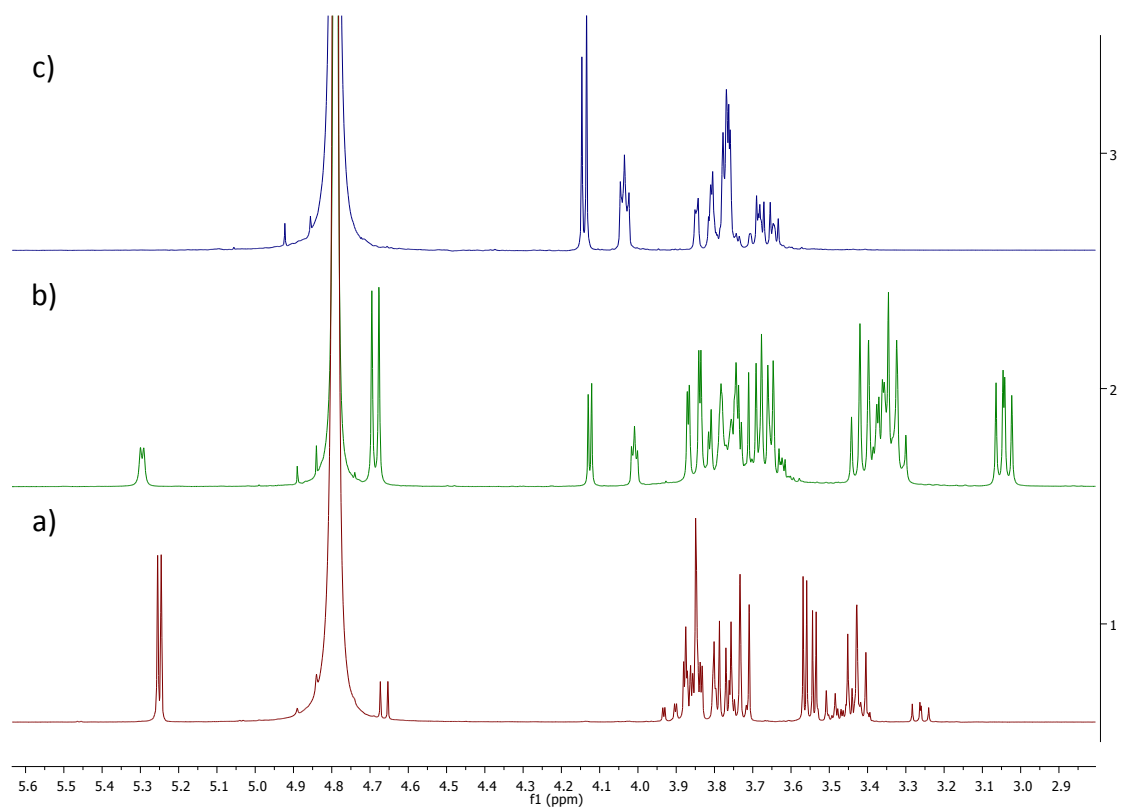


^{19}F NMR spectrum of complex $\text{IrCp}^*(\text{NHC})(\text{H}_2\text{O})_2$ (**3**) in D_2O :



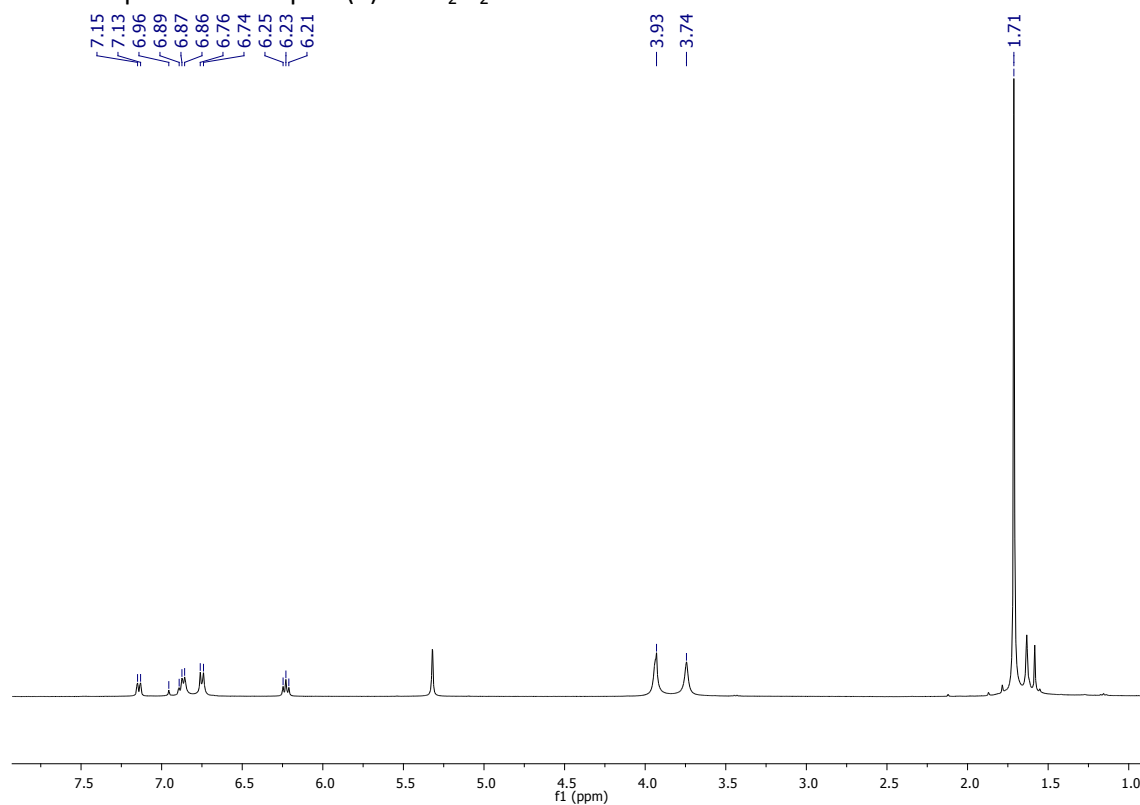
S2.4 ^1H NMR spectra of Glucose, Gluconic acid and the mixture in basic D_2O .

^1H -NMR of a) glucose, b) crude reaction after 2h showing partial conversion of glucose in gluconic acid and c) gluconic acid in basic D_2O (NaOH):

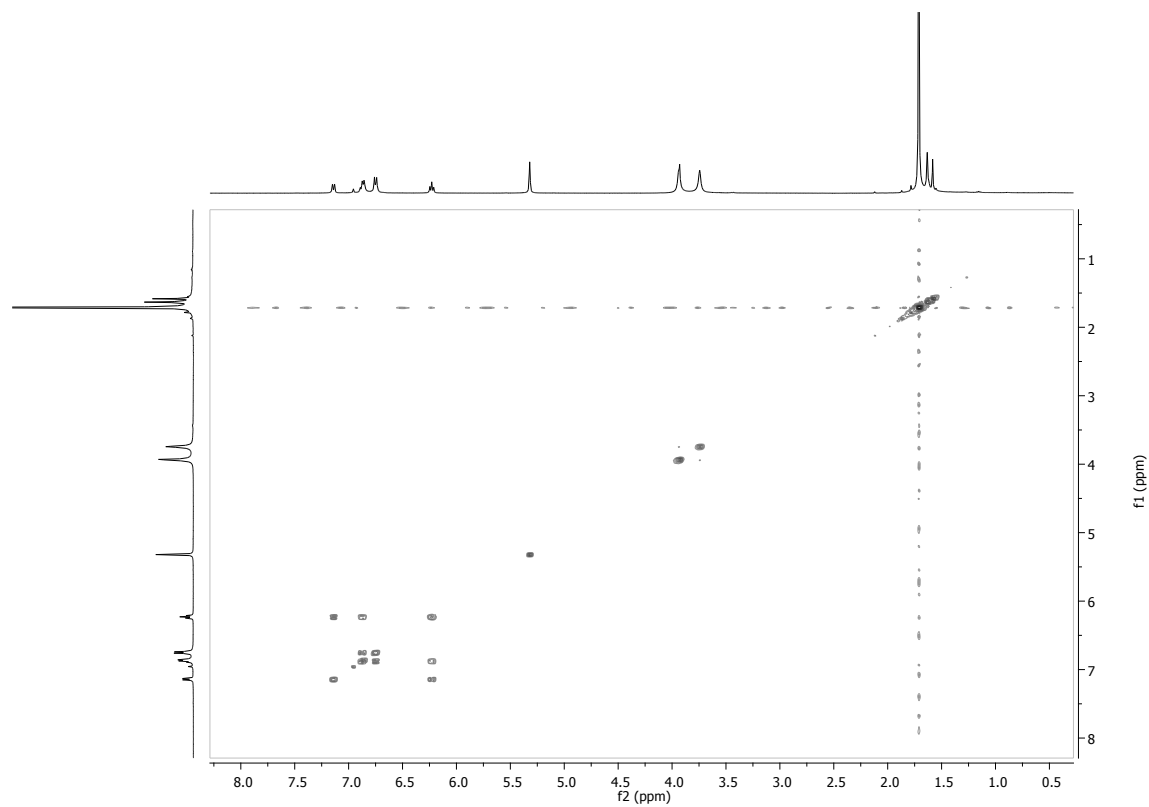


S2.5 NMR characterization of complex (4).

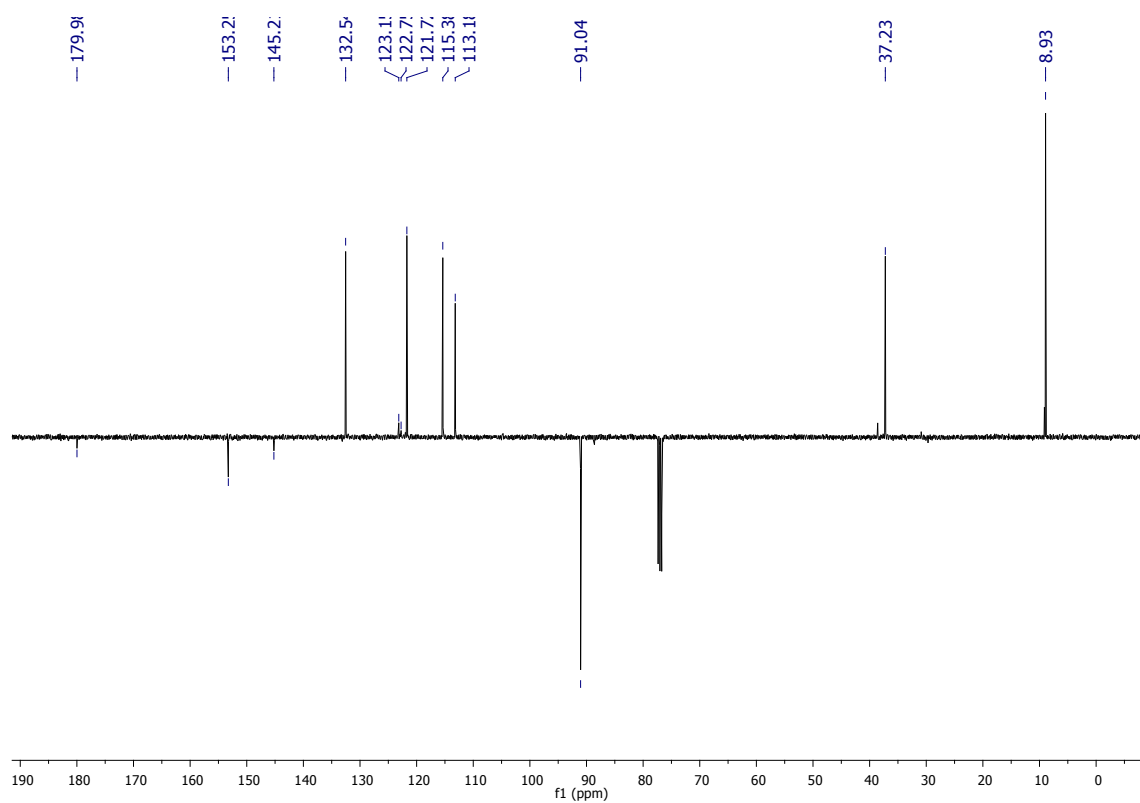
^1H NMR spectra of complex (4) in CD_2Cl_2 :



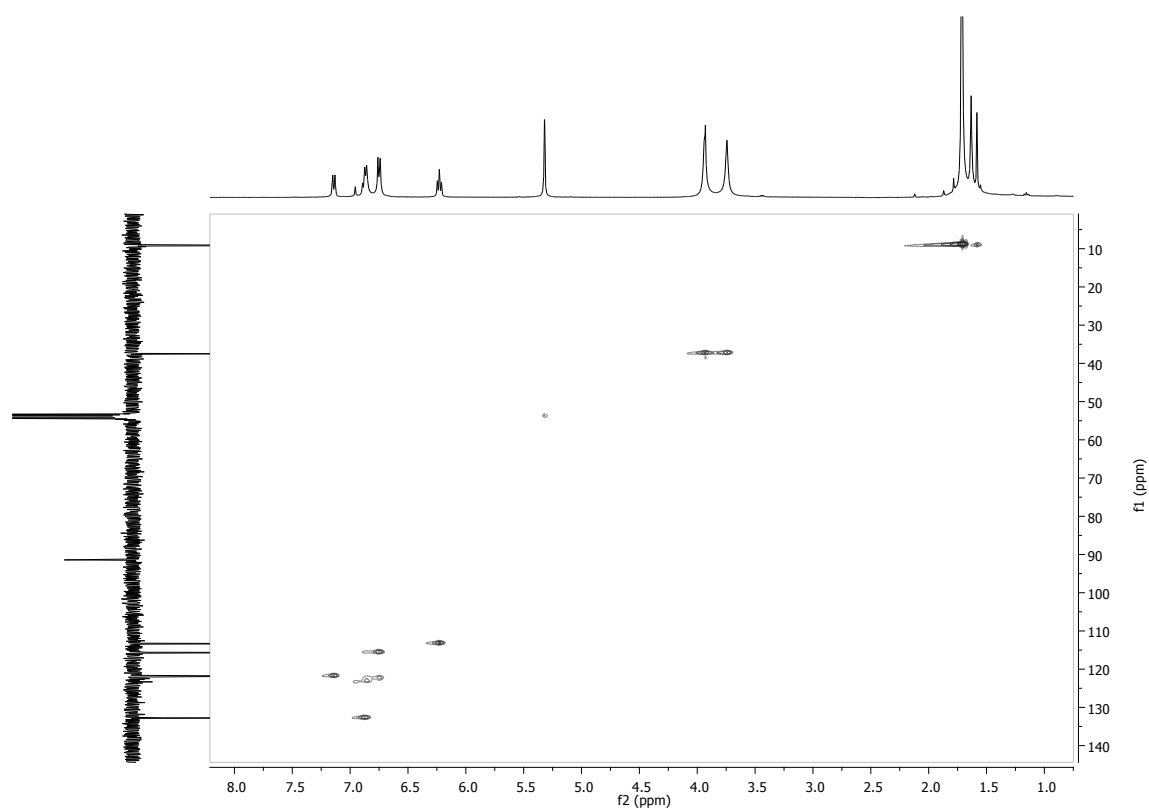
^1H - ^1H -COSY of complex (4) in CD_2Cl_2 :



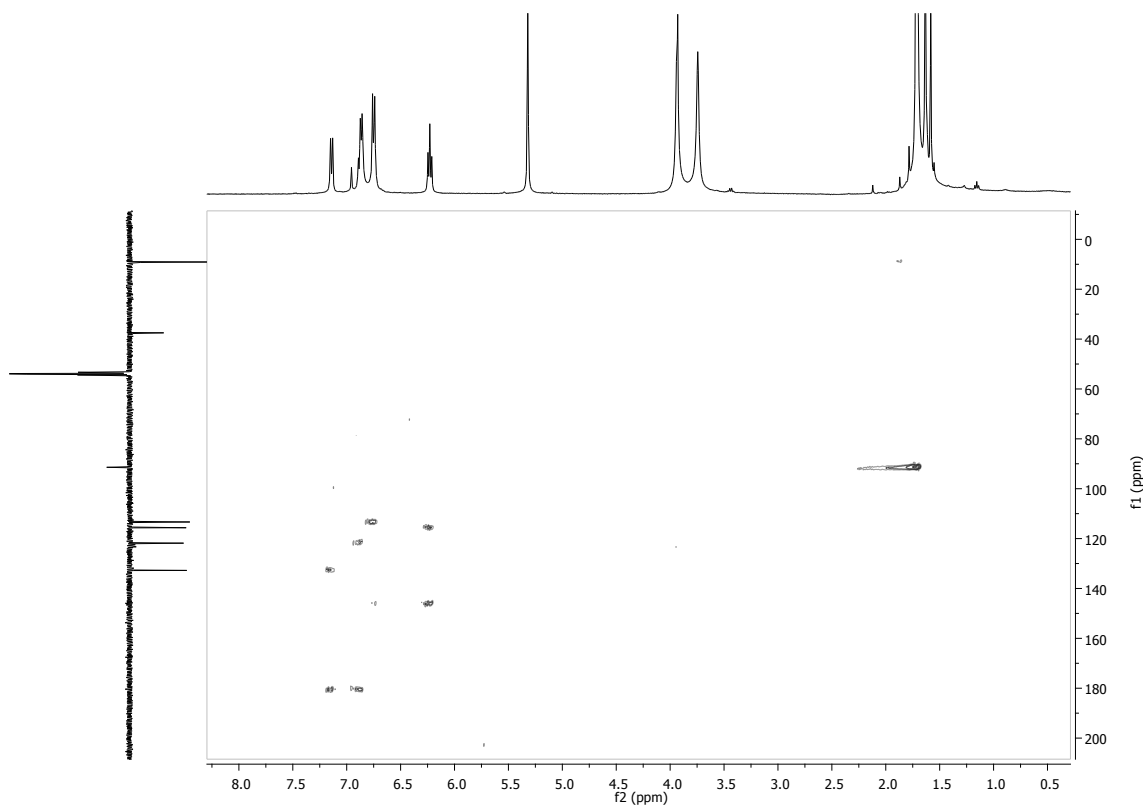
APT of complex (4) in CDCl₃:



¹H-¹³C-HSQCed of complex (4) in CD₂Cl₂:



^1H - ^{13}C -HMBC of complex (4) in CD_2Cl_2 :



S3. HPLC-ESI-MS/MS method for the quantification of glucose and gluconic acid

Another goal of the present work was to develop an analytical methodology combining the advantages of UHPLC-MS/MS with ESI tandem MS triple quadrupole for the rapid and reliable determination of glucose and gluconic acid in the tested catalytic runs. The applicability of the method and its high-throughput characteristics were demonstrated to obtain detailed reaction profiles and to optimize reaction conditions. We initially adapted previous analytical methods for the determination of glucoseⁱ and gluconic acidⁱⁱ in different commodities by HPLC-ESI-MS/MS.

S3.1. Preparation of the calibration standards

Glucose and gluconic acid (50%wt) were purchased from Alfa Aesar (Madrid, Spain). Standard stock solution containing both compounds were freshly prepared at 1000 mg/L in water:methanol (50:50). Intermediate solution (50 mg/L) was prepared by dilution of the stock solution 20-fold with water:methanol (95:5), and was used for preparation of the aqueous calibration standards and for spiking samples in the matrix effect study. HPLC-grade methanol (MeOH), formic acid (HCOOH , content >98%) were purchased from Scharlab (Barcelona, Spain). HPLC grade water was obtained from distilled water passed through a Milli-Q water purification system (Millipore, Bedford, MA, USA).

S3.2. Instrumentation, MS/MS optimization and chromatography

A Waters Acquity UPLC system was interfaced to a triple quadrupole mass spectrometer Xevo TQS (Waters) equipped with an orthogonal Z-spray electrospray ionization interface (ESI). Cone gas as well as desolvation gas was nitrogen set up 250 L/h and 1200 L/h, respectively. For operation in the MS/MS mode, collision gas was argon at 0.15 mL/min producing a pressure of 4×10^{-3} mbar in the collision cell. Other optimized parameters were: capillary voltages 2.0 kV (ESI-); source temperature 150 °C and desolvation temperature 650 °C; dwell time 50 ms. Full-scan and MS/MS spectra of the analytes were obtained from the infusion of individual 1 mg/L water:methanol (95:5) solutions of each compound at a flow rate of 20 $\mu\text{L min}^{-1}$ using a syringe pump. Like previous reports for the determination of glucoseⁱ and gluconic acidⁱⁱ by HPLC-ESI-MS/MS, both analytes were conveniently analysed by ESI ionization in the negative mode. Full-scan mass spectra displayed in both cases the $[\text{M} - \text{H}]^-$ ion as the base peak and were acquired in order to obtain the optimum cone voltage. Furthermore, product ion scan at different collision energies was carried out to determine the most abundant product ion for each compound for quantification purposes. Applied cone voltages and collision energies for glucose and gluconic acid are summarized in Table S1. The most abundant was used for quantification (Q) whereas the other transition was acquired for confirmation (q) by the comparison of the ion ratios of the two transitions (quantification and confirmation), with those obtained using standards. All data were acquired and processed using MassLynx and TargetLynx v 4.1 software (Waters).

Table S1. Analyte MS parameters used in the present work

Analyte	Transition	MRM transition	Cone voltage (V)	Collision energy (eV)
Glucose	Q	179.1 > 89.0	25	10
	q	179.1 > 59.0	25	15
Gluconic acid	Q	195.1 > 129.0	20	10
	q	195.1 > 75.0	20	15

Chromatography separation was performed using an Acquity UPLC HSS T3 1.8 μm particle size analytical column 2.1 x 100 mm (Waters). The mobile phases used were A = H_2O with 0.01% HCOOH and B = MeOH. The percentage of organic modifier (B) was kept constant for 3 minutes and then changed linearly as follows: 5 to 45 % from minute 3 to 5; 45% 6 min.; 45 to 5 % from minute 6 to 6.5 and remained constant until the time reached 8 min. The flow rate was 0.3 mL/min. The column was kept at 40 °C. The sample injection volume was 10 μL . At these conditions glucose and gluconic were eluted at 0.81 and 0.86 minutes, respectively. The linearity of the method was studied by analyzing standard solutions based on absolute responses in triplicate at 5 concentrations, in the range from 10 to 500 $\mu\text{g/L}$. Satisfactory linearity was obtained as judged by the correlation coefficient (r) higher than 0.99. Illustrative traces are shown in figure S1.

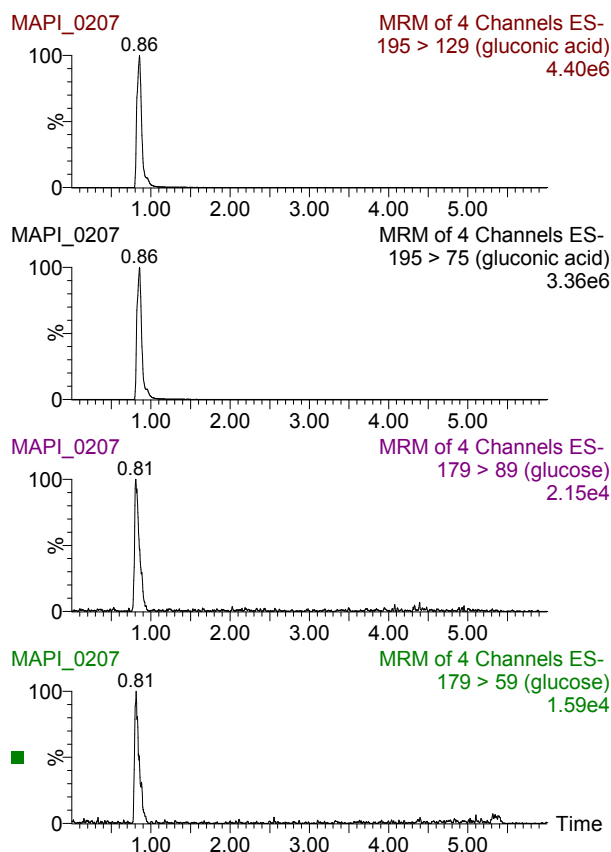


Figure S1. MRM chromatograms of 0.5 mg/L standards of glucose and gluconic acid.

S3.3. Study of matrix effects

The presence of matrix components can affect the ionization of the target compounds, reducing or enhancing the response compared with the pure compounds dissolved in solvents. In the present case, different additives (H_2SO_4 , HCl or NaOH) and catalyst loadings were used in the catalytic experiments and we investigate potential matrix effects in the determination of glucose and gluconic acid. Solutions containing additives and catalyst at catalytic conditions were spiked at different concentration levels with glucose and gluconic acid and the recoveries were analyzed. We found that the most critical factor to achieve satisfactory recoveries was the dilution step of the crude reaction.ⁱⁱⁱ For example, aliquots of 250 μL were taken from the reaction mixture (spiked at the working amount of substrates, namely 4000 mg/L) and were diluted from 4000 to 8000, (that results in solutions from 1 mg/L to 0.5 mg/L). The HPLC-MS-MS analysis of samples 4000-fold diluted displayed ion suppression effects as evidenced by the poor match between peak areas of spiked solutions and standards, in the absence of matrix, at the same concentration. Ion suppression was reduced by a performing a 8000-fold dilution of the crude samples. Under these conditions reproducible chromatography and detection limits ranging from 10 to 500 $\mu\text{g/L}$ for both compounds were obtained. Both glucose and gluconic acid were quantified by external calibration using absolute responses as matrix effects in the spiked samples tested were not much relevant.

S3.4. Sample preparation

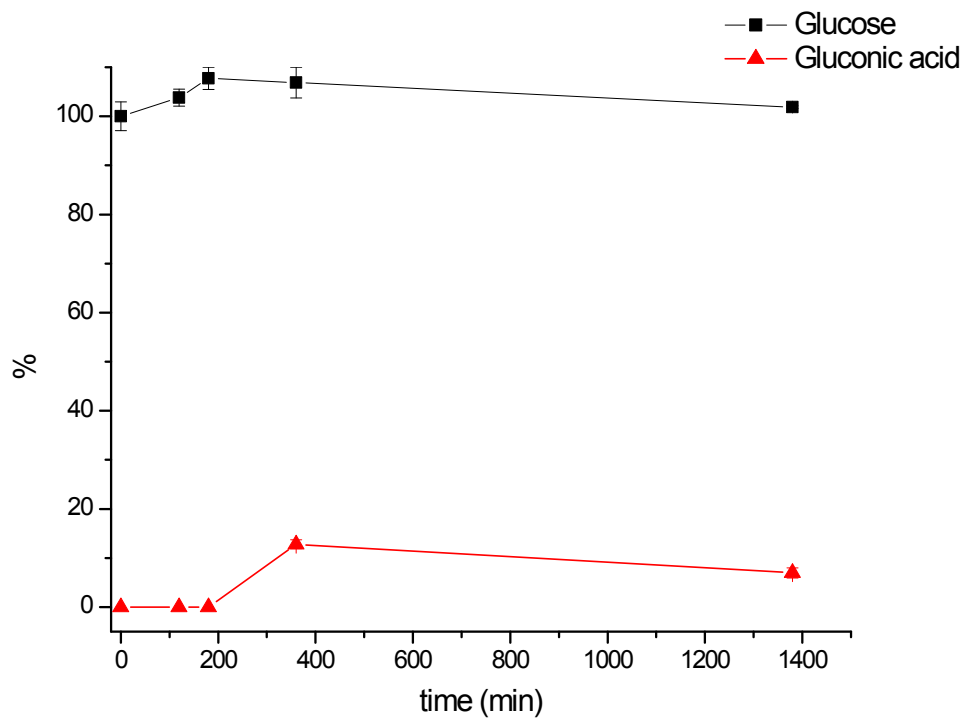
We aimed to create a robust method that comprise taking small aliquots of the crude reaction, diluting and injecting into the HPLC-MS system, the so called dilute-and-shoot procedure. When using a dilute-and-shoot approach, great care must be taken to ensure that matrix effects are minimized. We found that a previous dilution step of the crude reaction is crucial to overcome matrix effects, as described in the previous section. Hence, aliquots of 250 μ L were taken at different time intervals from the reaction mixture (the initial amount of glucose was 4000 mg/L) and were 8000 fold diluted. These aqueous samples were filtered using a 0.22- μ m membrane syringe filter (Agilent, USA) and 10 μ L were directly injected into the UPLC-MS/MS system by triplicate. Standard deviations in samples were below 15 % for glucose and 8 % for gluconic acid.

S3.5. References

- i) Monge, M. A., José J. Pérez, J. J., Dwivedi, P., Zhou, M., McCarty, N. A., Stecenko, A. A., Fernández, F. M.; *Rapid Commun. Mass Spectrom.* **2013**, *27*, 2263–2271
- ii) Sandín-España, P., Mateo-Miranda, M., López-Goti, C., De Cal, A., Alonso-Prados, J. L.; *Food Chemistry* **192** **2016**, 268–273
- iii) Dilution of samples can also minimize the shift in retention time; see for example F. Hernandez, J.V. Sancho, O.J. Pozo, C. Villaplana, M. Ibanez, S. Grimalt, J. AOAC Int. **86** **2003** 832.

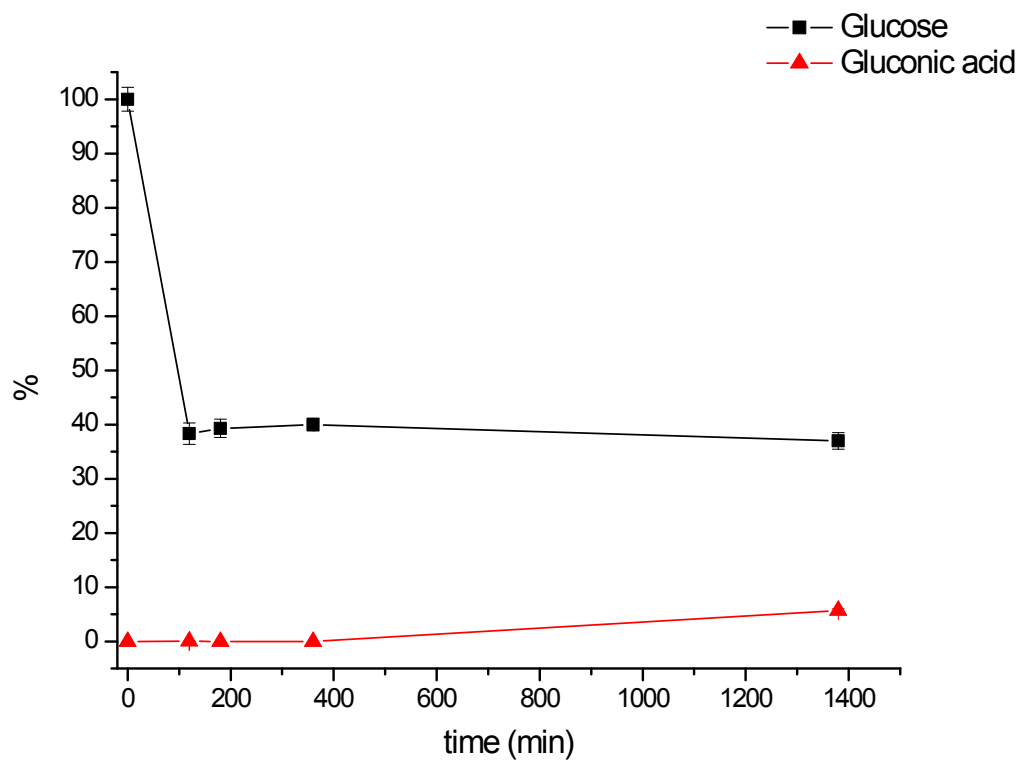
S3.6. HPLC reaction monitoring data of table 1.

Reaction monitoring by HPLC without catalyst and 1 eq. of H₂SO₄ (entry 1, table 1):

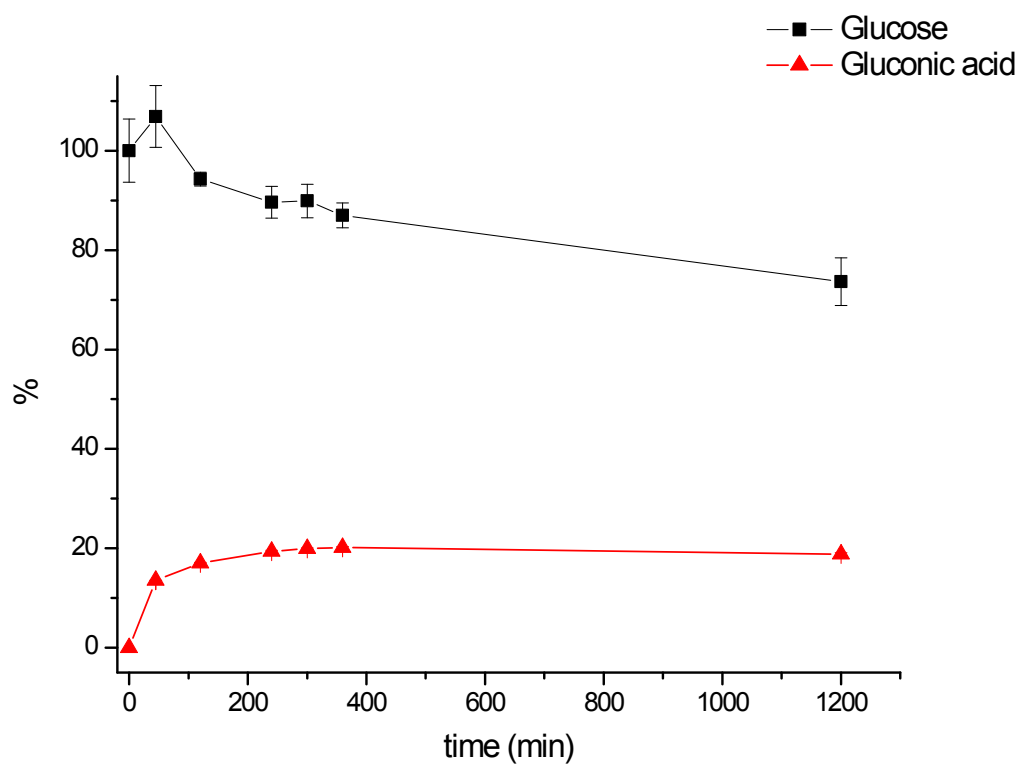


Rea

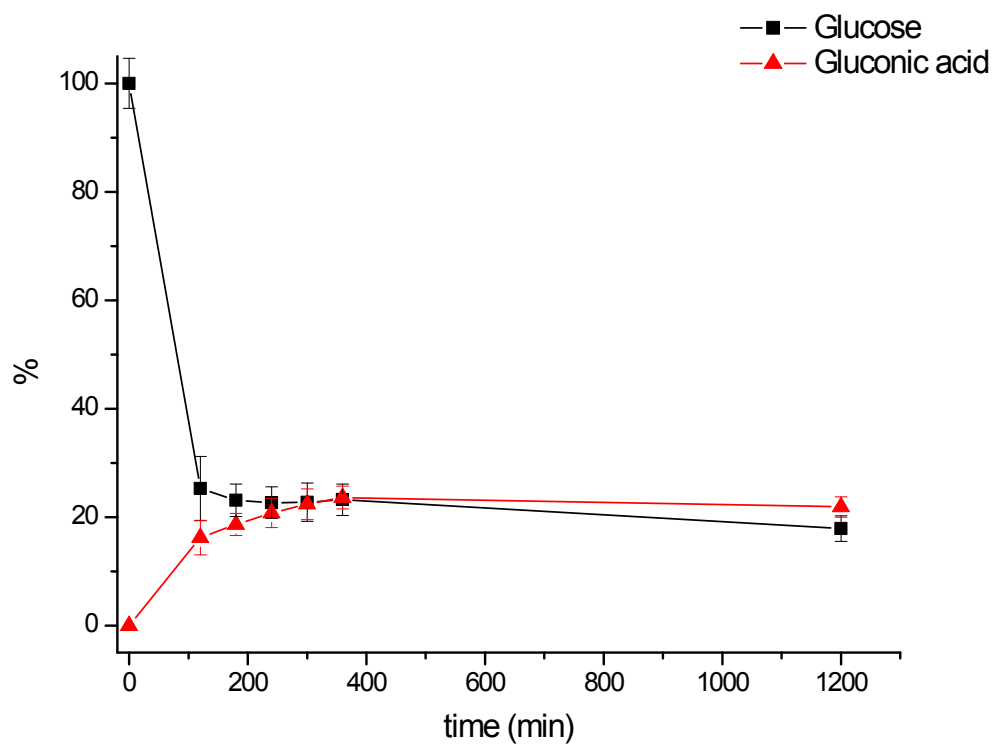
tion monitoring by HPLC without catalyst and 1 eq. of NaOH (entry 2, table 1):



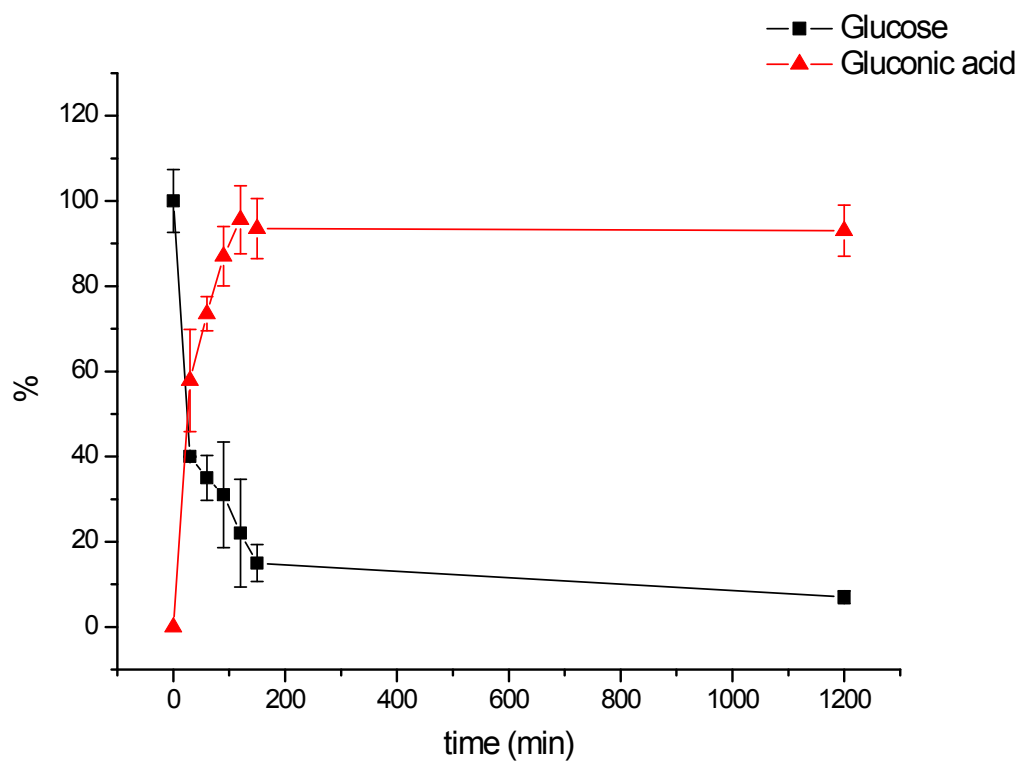
Reaction monitoring by HPLC using catalyst **2** and no additives (entry 4, table 1):



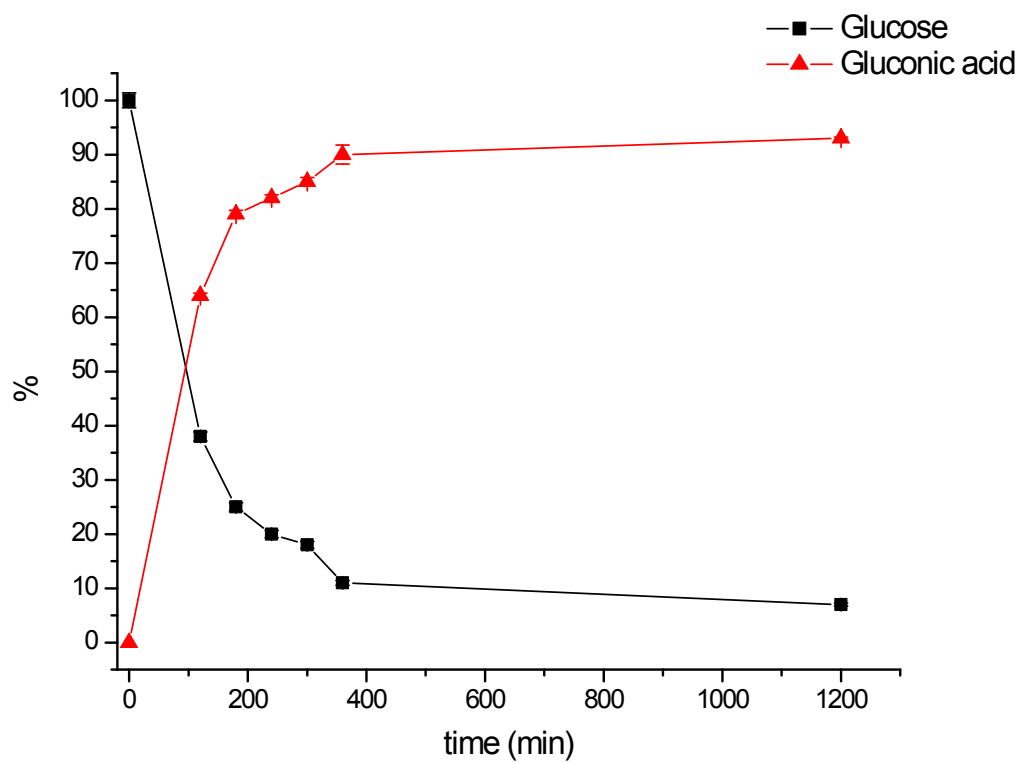
Reaction monitoring by HPLC using catalyst **1** and 1 eq. of NaOH (entry 5, table 1):



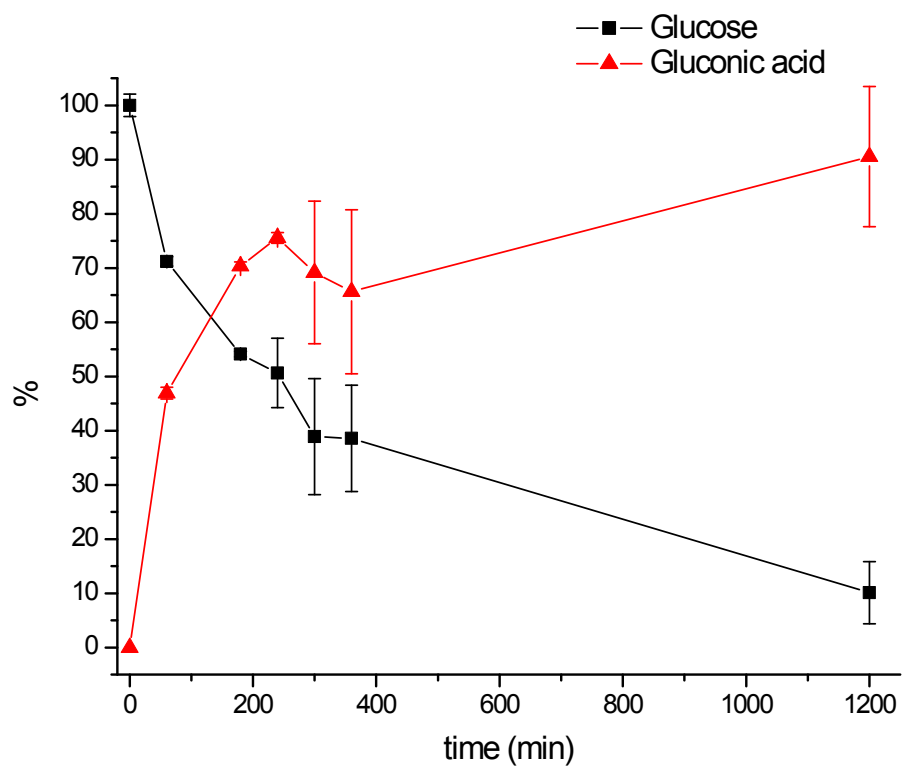
Reaction monitoring by HPLC using catalyst **1** and 1 eq. of H₂SO₄ (entry 7, table 1):



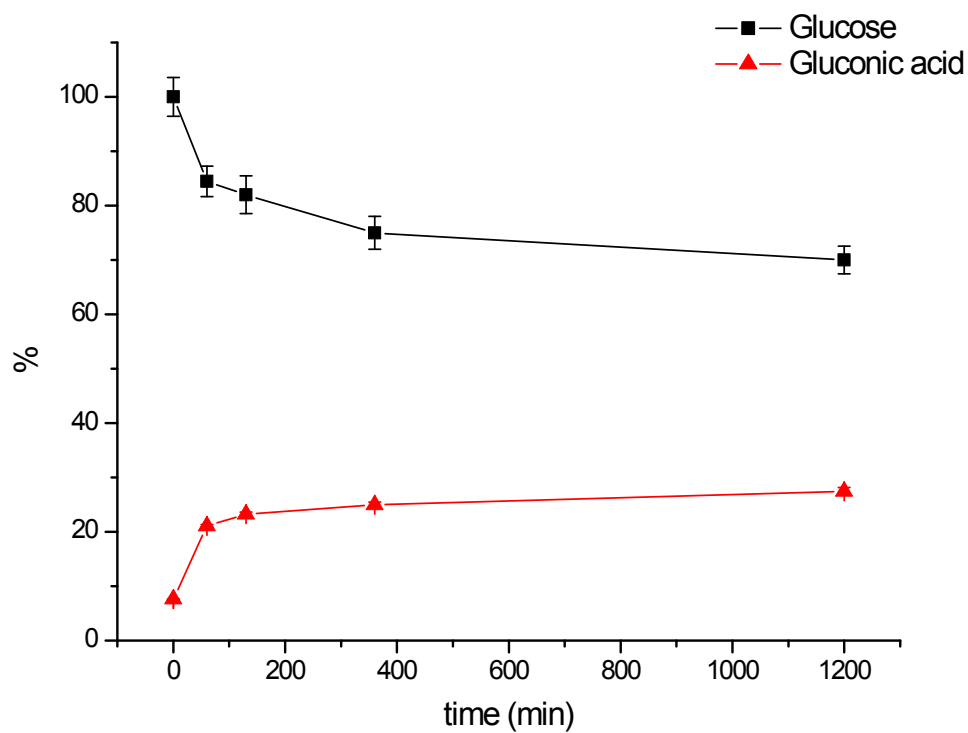
Reaction monitoring by HPLC using catalyst **1** and 0.75 eq. of H₂SO₄ (entry 8, table 1):



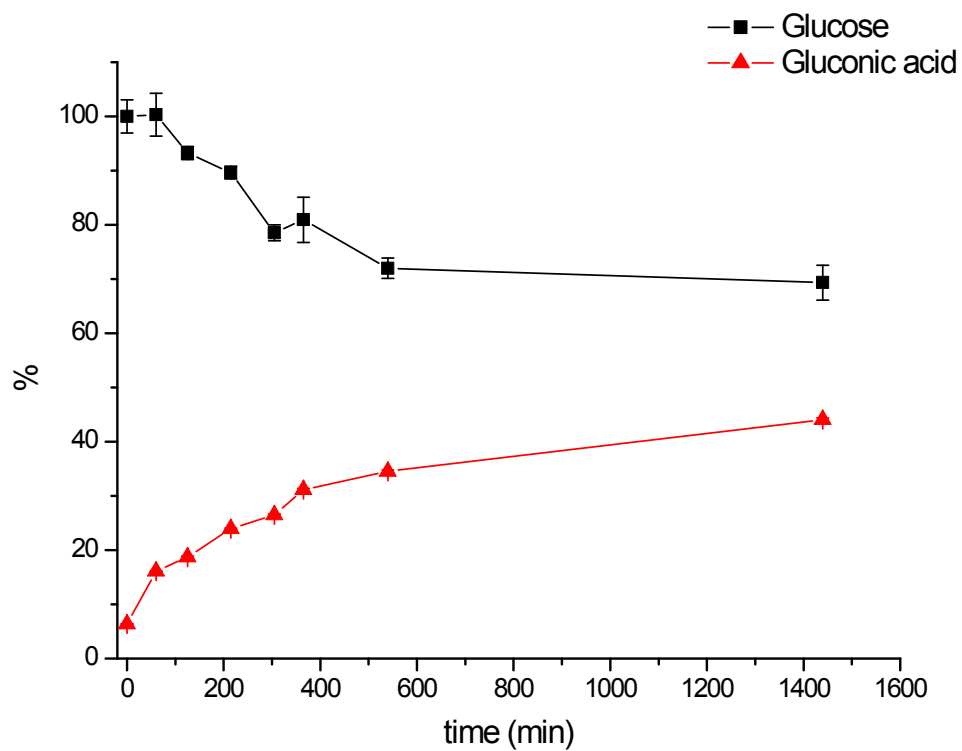
Reaction monitoring by HPLC using catalyst **1** and 0.5 eq. of H₂SO₄ (entry 9, table 1):



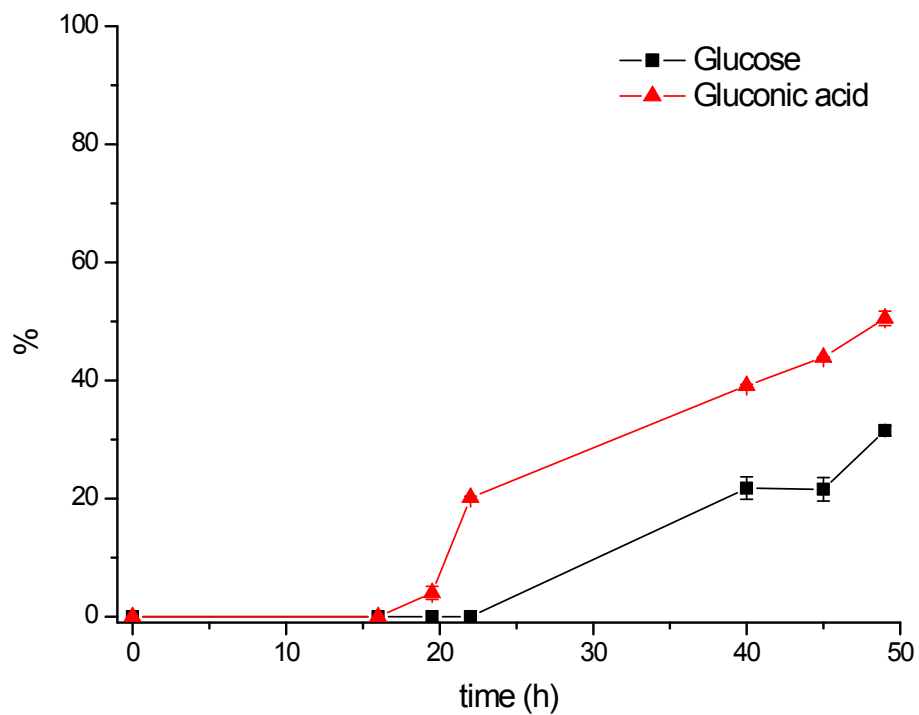
Reaction monitoring by HPLC using catalyst **2** and 0.5 eq. of H₂SO₄ (entry 12, table 1):



Reaction monitoring by HPLC using catalyst **2** and 0.25 eq. of HCl (entry 13, table 1):

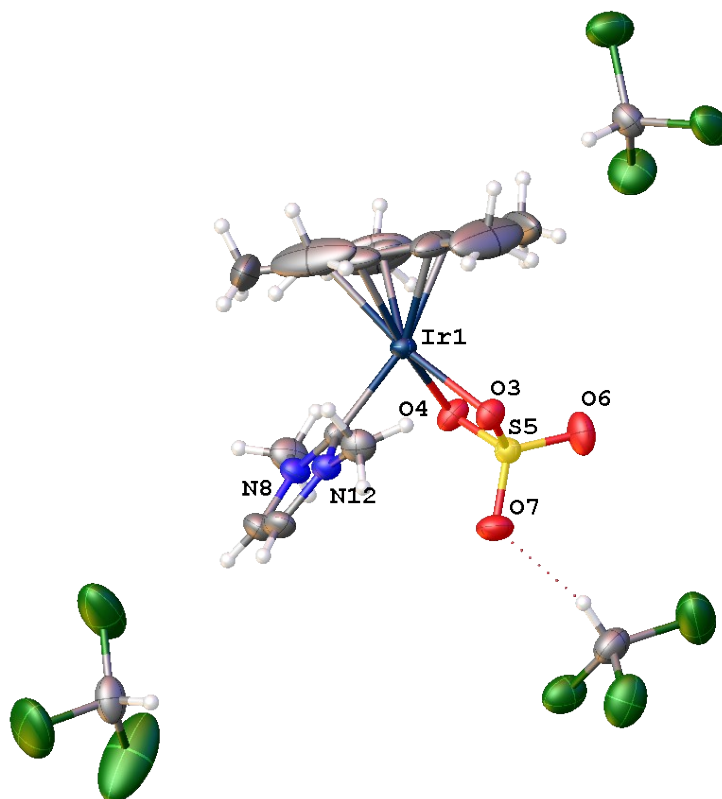


Reaction monitoring by HPLC using catalyst **1** and 1 eq. of H₂SO₄ (Figure 2):



S4. X-Ray Diffraction Studies

Crystallographic data and structure refinement for complex **2**.



Molecular diagram of compound **2**. Ellipsoids are at 50% probability level. Selected bond lengths [Å] and angles [°]: Ir(1) - C(2) 2.040(5), Ir(1) - O(3) 2.159(3), Ir(1) - O(4) 2.148(3), Ir(1) - Cp*_{cent} 1.78, O(3) - Ir(1) - O(4) 66.18(12), O(3) - Ir(1) - C(2) 85.92(16).

Table S2 Crystal data and structure refinement for 2.

Identification code	str2042
Empirical formula	C ₁₈ H ₂₆ Cl ₉ IrN ₂ O ₄ S
Formula weight	877.72
Temperature/K	199.9(4)
Crystal system	orthorhombic
Space group	Pbca
a/Å	11.2915(4)
b/Å	16.6242(6)
c/Å	32.7927(12)
α/°	90
β/°	90
γ/°	90
Volume/Å ³	6155.6(4)
Z	8
ρ _{calc} /g/cm ³	1.894
μ/mm ⁻¹	5.215
F(000)	3408.0
Crystal size/mm ³	0.353 × 0.276 × 0.162
Radiation	MoKα (λ = 0.71073)
2θ range for data collection/°	4.38 to 52.742
Index ranges	-10 ≤ h ≤ 14, -17 ≤ k ≤ 20, -40 ≤ l ≤ 39
Reflections collected	32939
Independent reflections	6277 [R _{int} = 0.0313, R _{sigma} = 0.0225]
Data/restraints/parameters	6277/0/323
Goodness-of-fit on F ²	1.065
Final R indexes [I ≥ 2σ (I)]	R ₁ = 0.0325, wR ₂ = 0.0791
Final R indexes [all data]	R ₁ = 0.0386, wR ₂ = 0.0845
Largest diff. peak/hole / e Å ⁻³	1.76/-1.26

Experimental

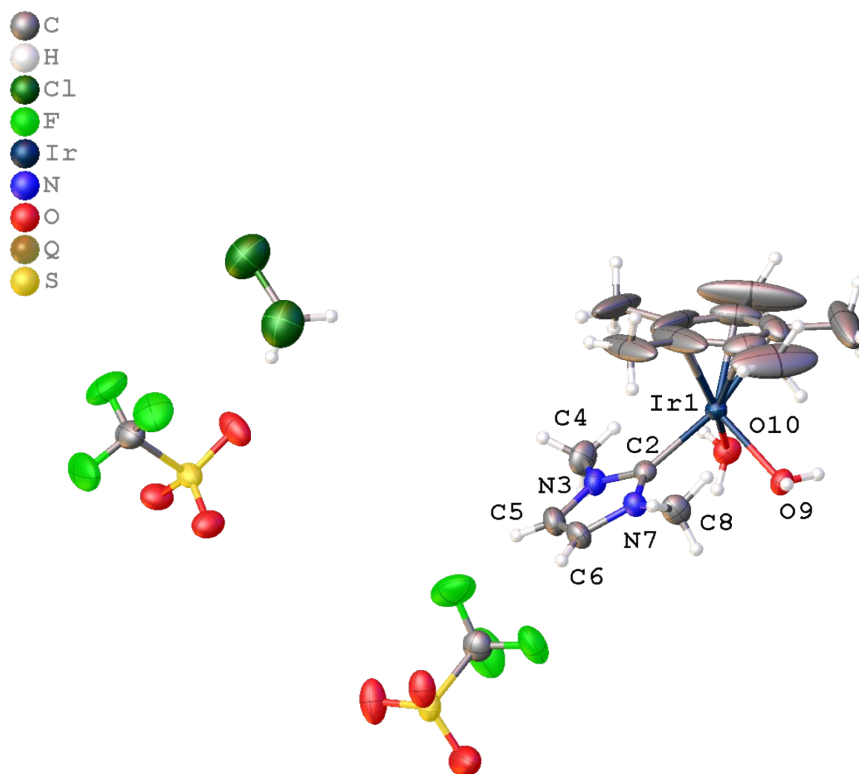
Single crystals of $C_{18}H_{26}Cl_9IrN_2O_4S$ complex **2** were mounted on a MicroMount[®] polymer tip (MiteGen) in a random orientation. Data collection was performed on a SuperNova dual source equipped with a CCD Atlas detector diffractometer (Agilent Technologies). The crystal was kept at 199.9(4) K during data collection. Using Olex2 [1], the structure was solved with the ShelXS [2] structure solution program using Direct Methods and refined with the ShelXL [3] refinement package using Least Squares minimisation.

1. Dolomanov, O.V., Bourhis, L.J., Gildea, R.J., Howard, J.A.K. & Puschmann, H. (2009), *J. Appl. Cryst.* 42, 339-341.
2. Sheldrick, G.M. (2008). *Acta Cryst.* A64, 112-122.
3. Sheldrick, G.M. (2015). *Acta Cryst.* C71, 3-8.

Crystal structure determination of **2**

Crystal Data for $C_{18}H_{26}Cl_9IrN_2O_4S$ ($M = 877.72$ g/mol): orthorhombic, space group *Pbca* (no. 61), $a = 11.2915(4)$ Å, $b = 16.6242(6)$ Å, $c = 32.7927(12)$ Å, $V = 6155.6(4)$ Å³, $Z = 8$, $T = 199.9(4)$ K, $\mu(\text{MoK}\alpha) = 5.215$ mm⁻¹, $D_{\text{calc}} = 1.894$ g/cm³, 32939 reflections measured ($4.38^\circ \leq 2\theta \leq 52.742^\circ$), 6277 unique ($R_{\text{int}} = 0.0313$, $R_{\text{sigma}} = 0.0225$) which were used in all calculations. The final R_1 was 0.0325 ($I > 2\sigma(I)$) and wR_2 was 0.0845 (all data).

Crystallographic data and structure refinement for complex **3**.



Molecular diagram of compound **3**. Ellipsoids are at 50% probability level. Selected bond lengths [Å] and angles [°]: Ir(1) - C(2) 2.060(4), Ir(1) - O(9) 2.176(3), Ir(1) - O(10) 2.172(3), Ir(1) - Cp*_{cent} 1.78, O(9) - Ir(1) - O(10) 81.19(12), O(9) - Ir(1) - C(2) 89.13(14).

Table S3 Crystal data and structure refinement for complex 3.

Identification code	str2049
Empirical formula	C ₁₈ H ₂₉ Cl ₂ F ₆ IrN ₂ O ₈ S ₂
Formula weight	842.65
Temperature/K	200.00(10)
Crystal system	monoclinic
Space group	P2 ₁ /c
a/Å	11.2529(5)
b/Å	21.6653(7)
c/Å	12.9575(5)
α/°	90
β/°	111.582(5)
γ/°	90
Volume/Å ³	2937.6(2)
Z	4
ρ _{calc} /cm ³	1.905
μ/mm ⁻¹	4.950
F(000)	1648.0
Crystal size/mm ³	0.568 × 0.101 × 0.081
Radiation	MoKα (λ = 0.71073)
2θ range for data collection/°	5.056 to 52.742
Index ranges	-14 ≤ h ≤ 14, -27 ≤ k ≤ 27, -16 ≤ l ≤ 16
Reflections collected	58882
Independent reflections	5992 [R _{int} = 0.0493, R _{sigma} = 0.0216]
Data/restraints/parameters	5992/24/344
Goodness-of-fit on F ²	1.059
Final R indexes [I >= 2σ (I)]	R ₁ = 0.0302, wR ₂ = 0.0739
Final R indexes [all data]	R ₁ = 0.0343, wR ₂ = 0.0769
Largest diff. peak/hole / e Å ⁻³	1.72/-1.39

Experimental

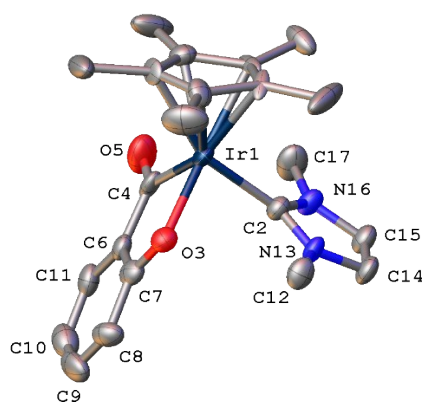
Single crystals of $C_{18}H_{29}Cl_2F_6IrN_2O_8S_2$ complex **3** were mounted on a MicroMount[®] polymer tip (MiteGen) in a random orientation. Data collection was performed on a SuperNova, Dual, Cu at zero, Atlas diffractometer (Agilent Technologies). The crystal was kept at 200.00(10) K during data collection. Using Olex2 [1], the structure was solved with the olex2.solve [2] structure solution program using Charge Flipping and refined with the ShelXL [3] refinement package using Least Squares minimisation.

1. Dolomanov, O.V., Bourhis, L.J., Gildea, R.J., Howard, J.A.K. & Puschmann, H. (2009), *J. Appl. Cryst.* 42, 339-341.
2. Bourhis, L.J., Dolomanov, O.V., Gildea, R.J., Howard, J.A.K., Puschmann, H. (2015). *Acta Cryst.* A71, 59-75.
3. Sheldrick, G.M. (2015). *Acta Cryst.* C71, 3-8.

Crystal structure determination of complex **3**

Crystal Data for $C_{18}H_{29}Cl_2F_6IrN_2O_8S_2$ ($M = 842.65$ g/mol): monoclinic, space group $P2_1/c$ (no. 14), $a = 11.2529(5)$ Å, $b = 21.6653(7)$ Å, $c = 12.9575(5)$ Å, $\beta = 111.582(5)^\circ$, $V = 2937.6(2)$ Å³, $Z = 4$, $T = 200.00(10)$ K, $\mu(\text{MoK}\alpha) = 4.950$ mm⁻¹, $D_{\text{calc}} = 1.905$ g/cm³, 58882 reflections measured ($5.056^\circ \leq 2\theta \leq 52.742^\circ$), 5992 unique ($R_{\text{int}} = 0.0493$, $R_{\text{sigma}} = 0.0216$) which were used in all calculations. The final R_1 was 0.0302 ($I > 2\sigma(I)$) and wR_2 was 0.0769 (all data).

Crystallographic data and structure refinement for complex **4**



Molecular diagram of compound **4**. Ellipsoids are at 50% probability level. Selected bond lengths [Å] and angles [°]: Ir(1) - C(2) 2.035(6), Ir(1) - O(3) 2.091(4), Ir(1) - C(4) 2.023(7), C(4) - O(5) 1.242(8), Ir(1) - Cp*_{cent} 1.81, C(4) - Ir(1) - O(3) 80.4(2), O(3) - Ir(1) - C(2) 88.8(2).

Table S4 Crystal data and structure refinement compound 4.

Identification code	mp-325
Empirical formula	C ₂₂ H ₂₇ IrN ₂ O ₂
Formula weight	543.65
Temperature/K	293(2)
Crystal system	triclinic
Space group	P-1
a/Å	8.5920(2)
b/Å	10.2464(3)
c/Å	12.6648(3)
α/°	78.655(2)
β/°	82.445(2)
γ/°	67.017(3)
Volume/Å ³	1004.57(5)
Z	2
ρ _{calc} /cm ³	1.797
μ/mm ⁻¹	6.664
F(000)	532.0
Crystal size/mm ³	0.12 × 0.11 × 0.08
Radiation	MoKα (λ = 0.71073)
2θ range for data collection/°	5.368 to 54.994
Index ranges	-11 ≤ h ≤ 11, -13 ≤ k ≤ 13, -16 ≤ l ≤ 16
Reflections collected	18137
Independent reflections	4599 [R _{int} = 0.1091, R _{sigma} = 0.0757]
Data/restraints/parameters	4599/41/346
Goodness-of-fit on F ²	1.141
Final R indexes [I ≥ 2σ (I)]	R ₁ = 0.0399, wR ₂ = 0.0940
Final R indexes [all data]	R ₁ = 0.0494, wR ₂ = 0.1087
Largest diff. peak/hole / e Å ⁻³	1.75/-3.67

Experimental

Single crystals of $C_{22}H_{27}IrN_2O_2$ complex **4** were mounted on a MicroMount[®] polymer tip (MiteGen) in a random orientation. Data collection was performed on a Xcalibur, Sapphire3 diffractometer. The crystal was kept at 293(2) K during data collection. Using Olex2 [1], the structure was solved with the ShelXS [2] structure solution program using Direct Methods and refined with the ShelXL [3] refinement package using Least Squares minimisation.

1. Dolomanov, O.V., Bourhis, L.J., Gildea, R.J, Howard, J.A.K. & Puschmann, H. (2009), *J. Appl. Cryst.* 42, 339-341.
2. Sheldrick, G.M. (2008). *Acta Cryst.* A64, 112-122.
3. Sheldrick, G.M. (2015). *Acta Cryst.* C71, 3-8.

Crystal structure determination of complex **4**

Crystal Data for $C_{22}H_{27}IrN_2O_2$ ($M = 543.65$ g/mol): triclinic, space group P-1 (no. 2), $a = 8.5920(2)$ Å, $b = 10.2464(3)$ Å, $c = 12.6648(3)$ Å, $\alpha = 78.655(2)^\circ$, $\beta = 82.445(2)^\circ$, $\gamma = 67.017(3)^\circ$, $V = 1004.57(5)$ Å³, $Z = 2$, $T = 293(2)$ K, $\mu(\text{MoK}\alpha) = 6.664$ mm⁻¹, $D_{\text{calc}} = 1.797$ g/cm³, 18137 reflections measured ($5.368^\circ \leq 2\theta \leq 54.994^\circ$), 4599 unique ($R_{\text{int}} = 0.1091$, $R_{\text{sigma}} = 0.0757$) which were used in all calculations. The final R_1 was 0.0399 ($I > 2\sigma(I)$) and wR_2 was 0.1087 (all data).

S5. Electrospray Ionization Mass Spectrometry (ESI-MS) and Collision Induced Dissociation (CID) experiments.

ESI-MS studies were conducted on a QTOF Premier instrument with an orthogonal Z-spray-electrospray interface (Waters, Manchester, UK) operating in the W-mode at a resolution of ca. 15000 (FWHM). The drying and cone gas was nitrogen set to flow rates of 300 and 30 L/h, respectively. A capillary voltage of 3.5 kV was used in the positive ESI(+) scan mode. The cone voltage was adjusted to a low value (typically $U_c = 5\text{--}15$ V) to control the extent of fragmentation in the source region. Chemical identification of the Ir-containing species was facilitated by the characteristic isotopic pattern at natural abundance of Ir and it was carried out by comparison of the isotope experimental and theoretical patterns using the MassLynx 4.1. For CID experiments, the cations of interest were mass-selected using the first quadrupole (Q1) and interacted with argon in the T-wave collision cell at variable collision energies ($E_{\text{laboratory}} = 3\text{--}15$ eV). The ionic products of fragmentation were analyzed with the time-of-flight analyzer. The isolation width was 1Da and the most abundant isotopomer was mass-selected in the first quadrupole analyzer.

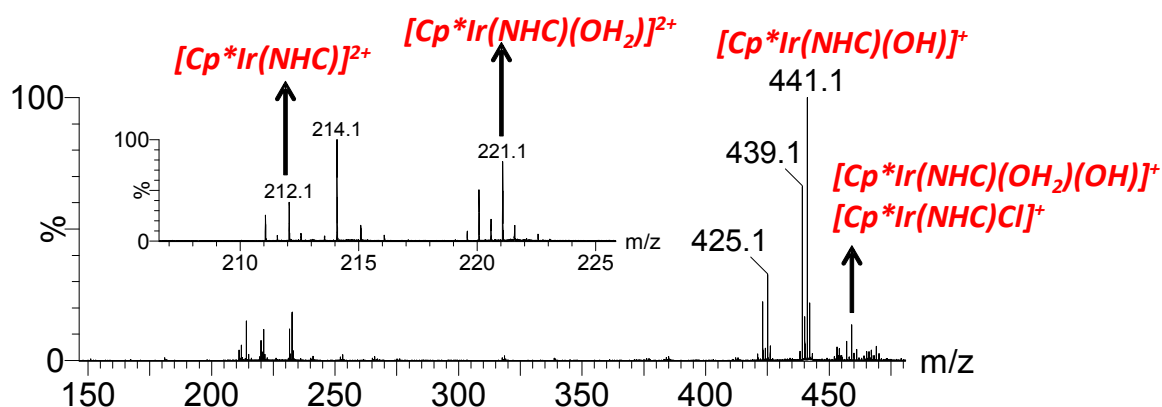


Figure S2. ESI mass spectrum of aqueous solutions of **1** recorded at low $U_c = 5$ V conditions. The inset shows the lower m/z region where doubly-charged species are observed. The peak at m/z 425.1 formally corresponds to $[\text{Cp}^*\text{Ir}(\text{NHC})\text{H}]^+$; however, the absence of any hydride signal in the ^1H NMR spectrum led us to consider this species as a product ion formed in the ESI chamber.

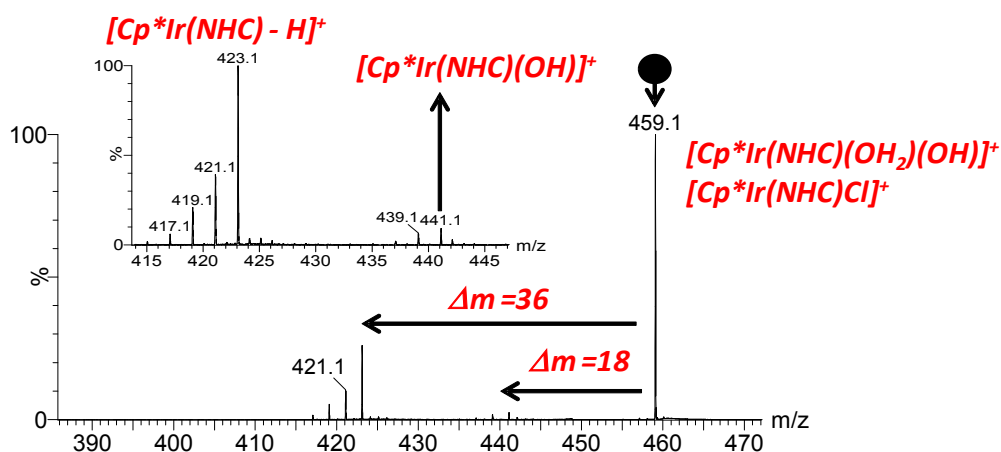


Figure S3. CID mass spectrum of mass-selected species at m/z 459 recorded at low collision energy $E_{lab} = 5$ eV showing the losses of $\Delta m = 18$ and 36 followed by consecutive H_2 liberation steps (for example the series of product ions at m/z 421, 419 and 417). The inset shows an expanded region in the m/z 415-446 range where the product ions are observed.

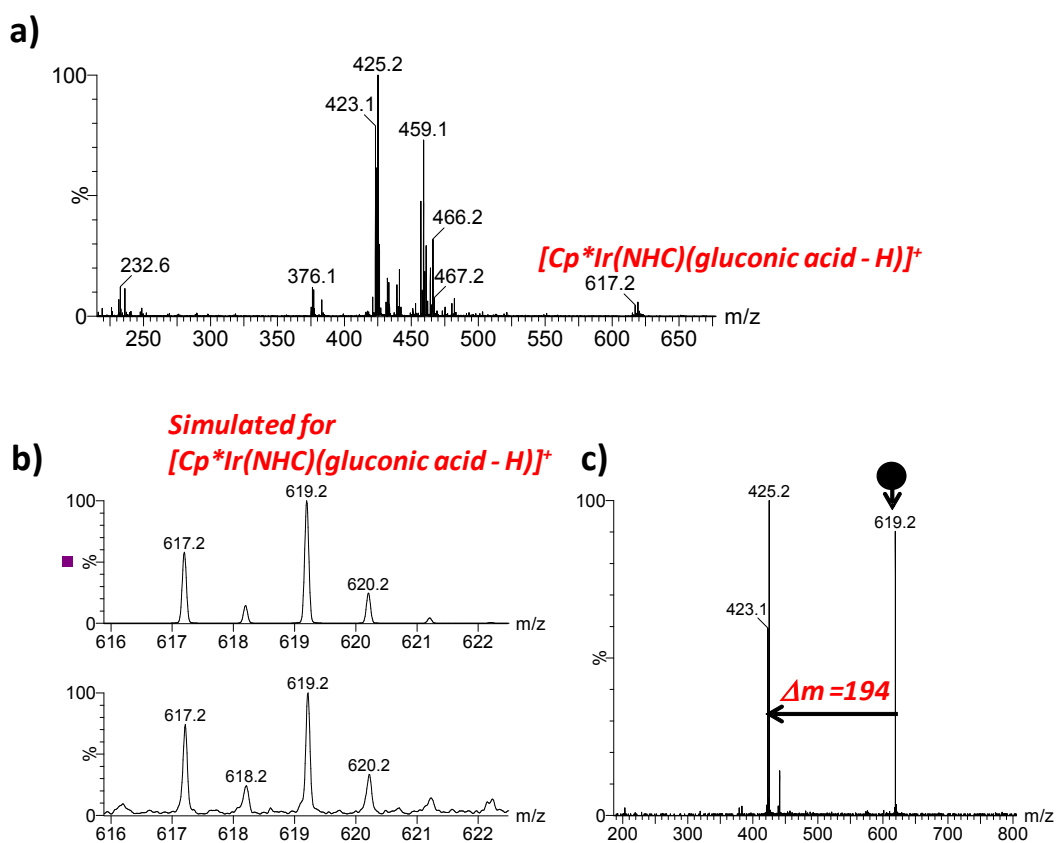


Figure S4. a) ESI mass spectrum of the catalytic reaction after 24 hours, diluted with water at $U_c = 5$ V; b) comparison between the calculated and experimental isotopic pattern for $[Cp^*Ir(NHC)(gluconic\ acid - H)]^+$ and c) CID mass spectrum of mass-selected species at m/z 619, $[Cp^*Ir(NHC)(gluconic\ acid - H)]^+$, recorded at low collision energy $E_{lab} = 15$ eV. It displays losses of $\Delta m = 194$ to yield a doubly-charged cation at m/z 423

S6. Speciation of complex **1** in H₂O by ¹H NMR spectroscopy.

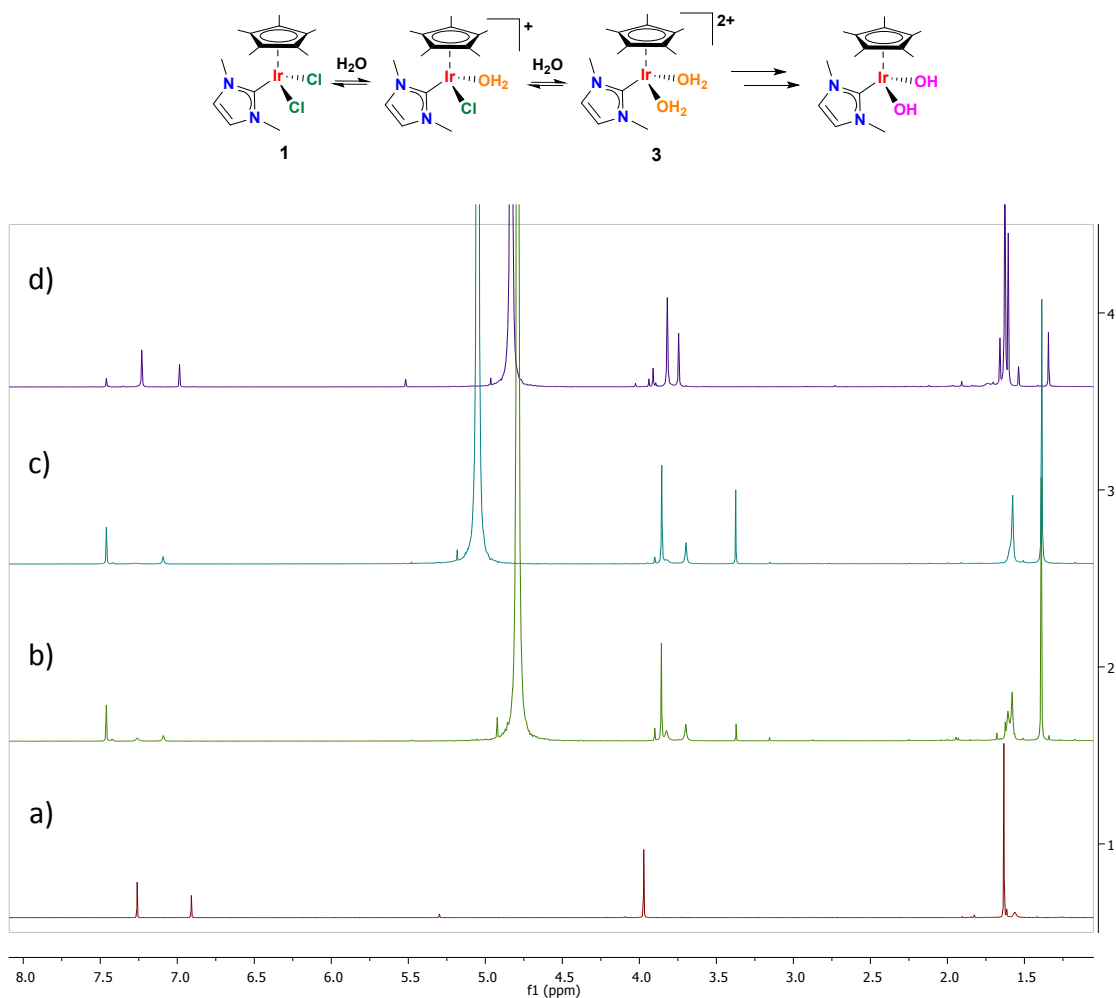


Figure S5. ¹H-NMR of complex **1** in D₂O: Presence of multiple sets and significant line broadening at room temperature is indicative of the co-existence of several species in equilibrium. a) ¹H-NMR of **1** in CDCl₃ (one set of signals) b) ¹H-NMR of **1** in D₂O c) ¹H-NMR of **1** in D₂O after the addition of a strong acid and d) ¹H-NMR of **1** in D₂O after the addition of a strong base.

S7. Density Functional Theory (DFT) calculations

S7.1 Computational details

Quantum mechanical calculations were performed with the Gaussian09 package¹ at the DFT/M06 level of theory.² SDD basis set and its corresponding effective core potentials (ECPs) were used to describe the Iridium atom.³ An additional set of f-type functions was also added.⁴ Carbon, nitrogen, oxygen and hydrogen atoms were described with a 6-31G** basis set.^{5,6} The open-chain form of D-glucose molecule has been modelled as R-2-hydroxypropanal. DFT studies have been complemented by calculations based on L-glucose and S-2-hydroxypropanal. All structures were freely optimized in water solution ($\epsilon = 78.3553$) by using the SMD continuum solvation model.⁷ Frequency calculations have been performed in order to determine the nature of the stationary points found (no imaginary frequencies for minima, only one imaginary frequency for transition states). A selection of DFT optimized geometries relevant for the discussion is included as an independent file entitled *DFT-structures.xyz*, which can be downloaded from the supplementary material section.

S7.2 Computational considerations

In order to obtain accurate reaction profiles one of the technical difficulties comes from the use of water as solvent and reagent in the catalytic reaction. This means that, whereas bringing one glucose molecule and one Iridium complex close together has an entropic cost to be computed, water is surrounding all of these molecules and therefore the processes in which a water molecule is participating has no entropic expense associated. Thus, in order to obtain reliable theoretical data, we have included two additional water molecules in the optimization of the different structures. This approach avoids the computation of entropic terms associated to the participation of water molecules in the different reaction steps.

The precise localization of TS1 is not straightforward, most probably due to the high number of freedom degrees present in the structure. As an alternative, a freeze-optimization-scan strategy has been performed. In this approach, the H-O distance was elongated in subsequent 0.05 Å steps and the structures were optimized using this geometrical restriction (Figure S6). Furthermore, this strategy was repeated by using 0.01 Å steps in the H-O distance range from 1.35 to 1.45 Å, the critical range in which the hydrogen transfer occurs. Such analysis afforded energy curves for the reaction coordinate connecting minima **I** and **III** and an estimation of the transition state structure (**TS1**), which shows a $d_{\text{O-H}}$ distance of 1.40 Å. A frequency calculation on this structure shows a unique negative frequency with an associated eigenvector fully consistent with the hydrogen transfer process.

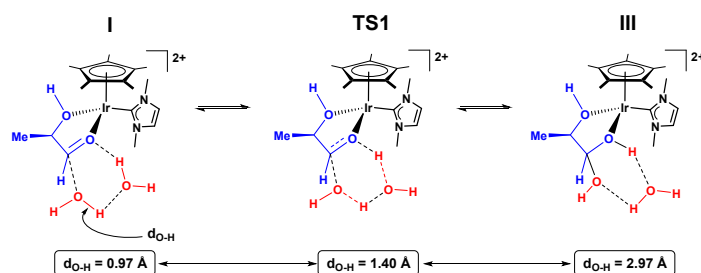


Figure S6. Freeze-optimization-scan strategy used for estimating the TS connecting I and III.

S7.3 Equilibria between iridium species present under the reaction conditions.

The presence of several nucleophilic species in the reaction media (water, glucose, and gluconic acid) which can coordinate to the IrCp*(NHC) moiety suggests that several equilibria might be operating in solution (figure S7). The position of these equilibria has been studied by DFT methods. The calculated ΔG° values for these equilibria are in a very narrow range ($\Delta G^\circ < 3$ kcal/mol), which is consistent with a system efficiently operating at a catalytic level.

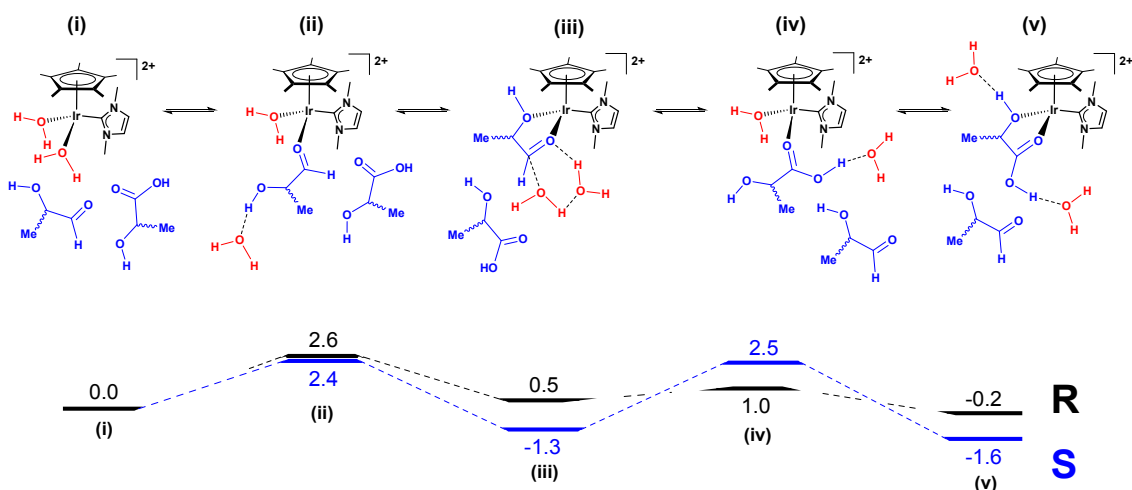


Figure S7. Equilibria and associated free energy barriers (kcal/mol) between different iridium complexes that can be formed under the reaction conditions.

S7.4 Mechanism proposal and calculated energy profile.

The mechanism proposal is based in three key experimental observations discussed in the manuscript: i) we have observed that the iridium-dichloride (**1**), iridium-sulphate (**2**), and the iridium-bisauquo (**3**) complexes are efficient catalysts in the dehydrogenation of glucose to gluconic acid. These results suggest that the complexes represent different forms of the catalysts and that the iridium-bisauquo (**3**) is itself involved in the catalytic cycle. The labile ligands in the Cp*Ir(NHC) fragment allow the bidentate coordination of glucose. ii) the results collected by ESI/MS confirm the formation of chelate iridium-glucose species upon dissociation of the labile ligands. These results reinforce the hypothesis of the [IrCp*(NHC)]²⁺ fragment as the catalyst's framework and the glucose-coordinated IrCp*(NHC) complex as the starting point of the cycle. iii) the catalytic results are improved in acidic media, which suggests a mechanism operating via doubly-charged species as the most likely one, over a mechanism operating via singly-charged species.

Based on the referred experimental observations and on previously reported results on metal-catalyzed oxidation of aldehydes to carboxylic acids, we propose the following reaction mechanism (Figure S8). The open-chain form of D-glucose molecule has been modelled as R-2-hydroxypropanal. The initial formation of a chelate (κ^2 -O,O) hydroxypropanal iridium complex (**I**) is followed by the water assisted O nucleophilic attack on the carbonyl C atom of the coordinated aldehyde (**II**, **TS1**). This process leads to a (κ^2 -O,O) 1,1,2-propanetriol iridium intermediate (**III**) which subsequently evolves to its (κ^2 -O,H) 1,1,2-propanetriol iridium isomer (**IV**). Then a concerted, water assisted, H⁺ transfer/H⁻ transfer by means of **V** (**TS2**) leads to the

formation of a hydride, (κ^1 -O) 2-hydroxypropanoic acid iridium species (**VI**) as well as one equivalent of H_3O^+ . The mixture subsequently gives rise to an iridium-dihydrogen intermediate (**VII**). At this point, several species might be formed (**VII**, **VIII**, **IX** and **X**) that, in a final step, release hydrogen and one equivalent of 2-hydroxypropanoic acid, therefore allowing the entry of a new molecule of 2-hydroxypropanal to the iridium coordination sphere (**XI** then **I**).

The DFT data predict the conversion of **IV** to **VI** via the **TS2** as the rate-determining step of the whole catalytic cycle. The calculated reaction profile in water solution (Figure S9) presents a free energy activation barrier of 26.3 kcal/mol, calculated as the free energy difference between **III** and **V**. This seems a reasonable value if we consider the experimental catalytic conditions (100°C, 20 h).

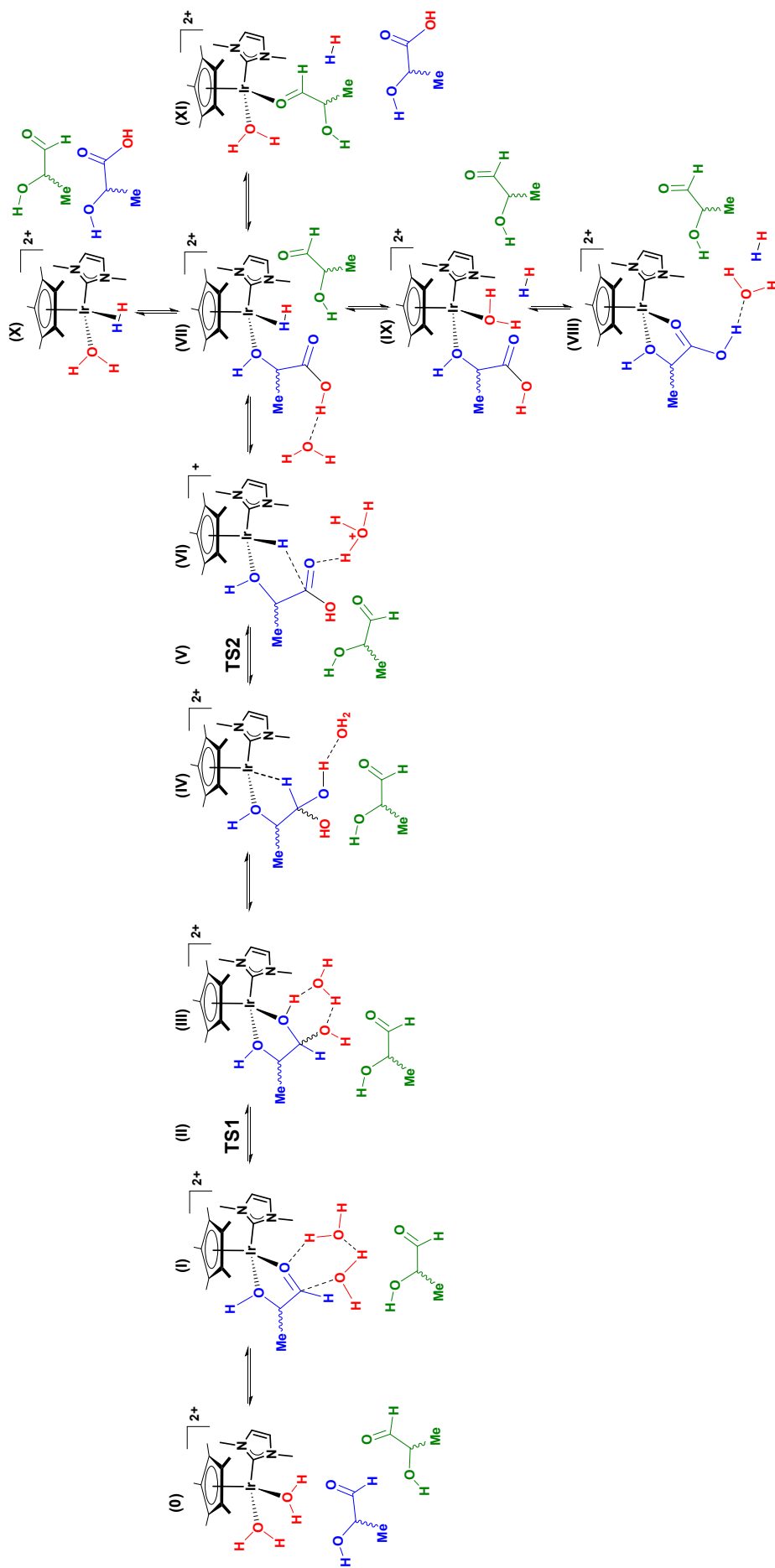


Figure S8. Mechanistic proposal for the conversion of MeCH(OH)CHO into the corresponding carboxylic acid catalyzed by [Cp*Ir(NHC)]²⁺.

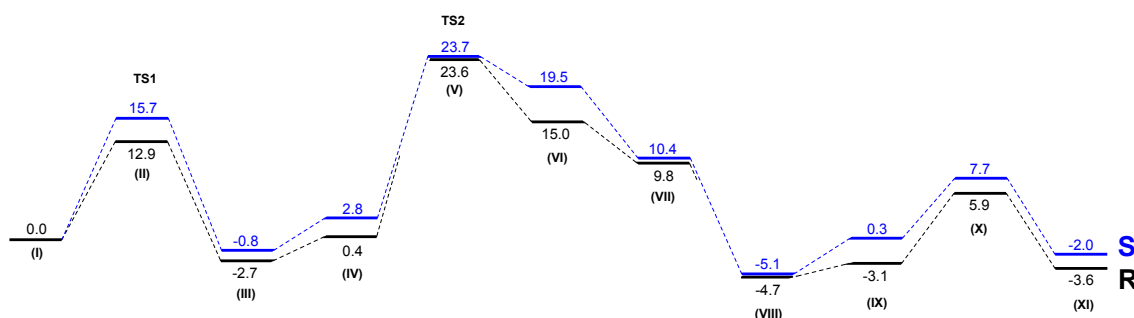


Figure S9. Free energy profile (kcal/mol) for both isomers (R and S) in the conversion of MeCH(OH)CHO into the corresponding carboxylic acid catalyzed by [Cp*Ir(NHC)]²⁺.

S7.5 References

- (1) Frisch, M. J.; Trucks, G. W.; Schlegel, H. B.; Scuseria, G. E.; Robb, M. A.; Cheeseman, J. R.; Scalmani, G.; Barone, V.; Mennucci, B.; Petersson, G. A.; Nakatsuji, H.; Caricato, M.; Li, X.; Hratchian, H. P.; Izmaylov, A. F.; Bloino, J.; Zheng, G.; Sonnenberg, J. L.; Hada, M.; Ehara, M.; Toyota, K.; Fukuda, R.; Hasegawa, J.; Ishida, M.; Nakajima, T.; Honda, Y.; Kitao, O.; Nakai, H.; Vreven, T.; Montgomery, J. A., Jr.; Peralta, J. E.; Ogliaro, F.; Bearpark, M.; Heyd, J. J.; Brothers, E.; Kudin, K. N.; Staroverov, V. N.; Keith, T.; Kobayashi, R.; Normand, J.; Raghavachari, K.; Rendell, A.; Burant, J. C.; Iyengar, S. S.; Tomasi, J.; Cossi, M.; Rega, N.; Millam, J. M.; Klene, M.; Knox, J. E.; Cross, J. B.; Bakken, V.; Adamo, C.; Jaramillo, J.; Gomperts, R.; Stratmann, R. E.; Yazyev, O.; Austin, A. J.; Cammi, R.; Pomelli, C.; Ochterski, J. W.; Martin, R. L.; Morokuma, K.; Zakrzewski, V. G.; Voth, G. A.; Salvador, P.; Dannenberg, J. J.; Dapprich, S.; Daniels, A. D.; Farkas, O.; Foresman, J. B.; Ortiz, J. V.; Cioslowski, J.; Fox, D. J. *Gaussian 09, Revision D.01*, Gaussian, Inc.: Wallingford CT, **2013**.
- (2) Zhao, Y.; Truhlar, D. G. *Theor. Chem. Acc.* **2008**, *120*, 215-241.
- (3) Andrae, D.; Häussermann, U.; Dolg, M.; Stoll, H.; Preuss, H. *Theor. Chim. Acta* **1990**, *77*, 123-141.
- (4) Ehlers, A. W.; Böhme, M.; Dapprich, S.; Gobbi, A.; Höllwarth, A.; Jonas, V.; Köhler, K. F.; Stegmann, R.; Veldkamp, A.; Frenking, G. *Chem. Phys. Lett.* **1993**, *208*, 111-114.
- (5) Harihara, P. C.; Pople, J. A. *Theor. Chim. Acta* **1973**, *28*, 213-222.
- (6) Francl, M. M.; Pietro, W. J.; Hehre, W. J.; Binkley, J. S.; Gordon, M. S.; Defrees, D. J.; Pople, J. A. *J. Chem. Phys.* **1982**, *77*, 3654-3665.
- (7) Marenich, A. V.; Cramer, C. J.; Truhlar, D. G. *J. Phys. Chem. B* **2009**, *113*, 6378-6396.